LncRNA LUCAT1 induced by *Helicobacter pylori* promotes M2 macrophage polarization via exosomal MIF in gastric cancer

Seo Yeon Kim

The Graduate School
Yonsei University
Department of Medical Science

LncRNA LUCAT1 induced by *Helicobacter pylori* promotes M2 macrophage polarization via exosomal MIF in gastric cancer

A Dissertation Submitted
to the Department of Medical Science
and the Graduate School of Yonsei University
in partial fulfillment of the
requirements for the degree of
Doctor of Philosophy in Medical Science

Seo Yeon Kim

January 2025

This certifies that the Dissertation of Seo Yeon Kim is approved

Thesis Supervisor Chul Hoon Kim

Thesis Committee Member Sang Kil Lee

Thesis Committee Member Ki Taek Nam

Thesis Committee Member Jae-Ho Cheong

Thesis Committee Member Minkyu Jung

The Graduate School
Yonsei University

January 2025

ACKNOWLEDGEMENTS

As I conclude my doctoral journey, I would like to express my heartfelt gratitude.

First and foremost, I would like to thank my advisor, Professor Sang Kil Lee, for giving me the opportunity to work on such an excellent research topic. With his warm guidance and teaching, I was able to complete my degree successfully. I am deeply grateful for the opportunity to have learned from him and conducted this research under his mentorship.

I also extend my sincere thanks to the members of my dissertation committee, who guided my thesis despite their busy schedules with clinical and research duties, and to Professor Da Hyun Jung, who has always supported and encouraged me with her close attention and mentorship.

I would also like to take this opportunity to thank those who helped me whenever I encountered difficulties during my studies. I am deeply thankful to the Ph.D. mentors in my lab, who provided invaluable assistance throughout the experiments and helped elevate the quality of my research.

Moreover, no one has been more important to me during this long and challenging doctoral journey than my family. I would like to express my gratitude to my parents, whose love and guidance have always been with me in everything I do. I am sincerely grateful for their unwavering belief in me and their steadfast support.

Throughout this journey, I have gained both perseverance and potential. Each new challenge required me to overcome obstacles, and I learned the importance of not giving up. However, I could not have navigated these times and challenges as smoothly without the support of those around me. For that, I would like to express my deepest thanks once again to all who helped me along the way.

TABLE OF CONTENTS

LIST OF FIGURES

LIST OF TABLES

ABSTRACT

LncRNA LUCAT1 induced by *Helicobacter pylori* promotes M2 macrophage polarization via exosomal MIF in gastric cancer

Helicobacter pylori (*H. pylori*) is a well-established etiological factor for the development of gastritis, peptic ulcer disease, and even gastric cancer (GC). Long noncoding RNAs (lncRNAs) are RNA molecules that are more than 200 nucleotides in length, are widely recognized for their critical role in the development and progression of various cancers, including GC. While it is known that lncRNAs are involved in cancer development following inflammatory responses, such as those triggered by *H. pylori*, knowledge regarding the changes in lncRNA expression specifically induced by *H. pylori* remains limited. To address this, I analyzed the changes in lncRNA and gene expression profiles in normal and GC cells upon *H. pylori* infection, considering *H. pylori*'s pathological factors, including oncoprotein cytotoxin associated gene A (CagA) and identify lncRNAs that contribute to *H. pylori*-infected GC progression. RNA sequencing and subsequent validation studies confirmed that LUCAT1 is markedly upregulated by CagA-positive *H. pylori*. This upregulation subsequently elevates the expression of macrophage migration inhibitory factor (MIF), which is secreted via exosomes. In turn, exosomal MIF promotes M2 polarization of tumor-associated macrophages, thereby potentiating GC cell malignancy. These findings underscore the profound impact of *H. pylori* infection on the tumor microenvironment through lncRNA expression and exosome-

mediated signaling regulation, highlighting the pivotal role of lncRNA-driven mechanisms in GC progression. This study offers an opportunity to explore therapeutic strategies that target lncRNA modulation and exosomal signaling in *H. pylori*, rather than focusing solely on its complete eradication.

Key words : *Helicobacter pylori*, CagA, long non-coding RNA, LUCAT1, MIF, macrophage, exosome, RNA-sequencing, gastric cancer

1. Introduction

Helicobacter pylori, a gram-negative microaerophilic bacterium, is widely recognized as the most serious risk factor for gastric cancer (GC).[1] *H. pylori* produces a well-recognized oncoprotein, cytotoxin-associated gene A (CagA)[2-4], which modulates various intracellular signaling pathways involved in GC development.[5] Furthermore, *H. pylori* infection can influence epigenetic regulation by altering the expression of noncoding RNAs, including microRNAs (miRNAs) and long noncoding RNAs (lncRNAs).[6-8]

H. pylori infection triggers an immune response that recruits macrophages to the gastric mucosa, where they secrete pro-inflammatory cytokines and chemokines, contributing to inflammation and tissue damage.[9-11] Depending on the micro-environmental signals macrophages encounter, they can differentiate into classically activated (M1) macrophages involved in pro-inflammatory and antitumor responses or alternatively activated (M2) macrophages associated with tissue remodeling, immune modulation, and tumor progression.[12-14] Tumor-derived factors, including exosomes, facilitate macrophage recruitment and polarization toward the M2 phenotype, thereby enhancing the metastatic potential.[15] Exosomes are 30–150 nm-diameter extracellular vesicles that play a critical role in intercellular communication by transporting various biomolecules, such as proteins, lipids, mRNAs, miRNAs, and lncRNAs.[16-18] Macrophage migration inhibitory factor (MIF), another key macrophage regulator, plays a crucial role in maintaining both innate and adaptive immunity. Aberrant MIF expression has been linked to various inflammatory diseases and cell cycle event dysregulation during carcinogenesis.[19] Specifically, increased

MIF expression, notably induced by CagA-positive *H. pylori*, is significantly associated with gastritis, gastric ulcer, and GC development.[20]

LncRNAs play a pivotal role in gene regulation, including chromatin remodeling, transcriptional control, and post-transcriptional modifications, and are particularly involved in tumorigenesis and progression following chronic inflammation.[21-23] Notably, the significance of lncRNAs has increased with growing insight into the diverse pathways through which they contribute *H. pylori*-induced gastric carcinogenesis.[24] However, whether lncRNAs are involved in regulating the tumor microenvironment (TME) in *H. pylori*-induced chronic inflammation leading to GC remains unclear.

LUCAT1, an lncRNA, is associated with the development of various cancers such as lung cancer, which was initially reported in 2013 due to smoking[25], as well as GC[26], esophageal[27], and bladder cancer.[28] Recent studies have emphasized its involvement in inflammatory response regulation and its association with inflammatory disease onset.[29,30] Furthermore, it drives epithelial–mesenchymal transition (EMT) within the extracellular matrix, a well-established mechanism in cancer initiation and progression.[31,32]

This study sought to uncover the role and underlying mechanisms of lncRNAs in the process by which *H. pylori* infection induces changes in macrophages and the TME within the gastric mucosa. To this end, various *H. pylori* strains and toxins were applied to gastric mucosal and cancer cells, followed by RNA sequencing to identify lncRNAs and genes and examine their effects on macrophages and the TME.

2. MATERIALS AND METHODS

2.1. Cell culture and bacteria supplementary materials

GC cell lines and normal cell line were purchased from the Korean Cell Line Bank (KCLB, SNU, Seoul, Korea) and the American Type Culture Collection (ATCC, Rockville, MD, USA). The human acute monocytic leukemia THP-1 cells were purchased from the American Type Culture Collection (ATCC). All cells were cultured at 37 ℃ in humidified atmosphere of 5% CO_2 using RPMI-1640 medium (Thermo Fisher Scientific, Rockford, IL, USA) supplemented with 10% fetal bovine serum (FBS) and 1% penicillin/streptomycin (Thermo Fisher Scientific). Differentiation of THP-1 cells into macrophage was performed by incubating the cells with 160 ng/Ml phorbol 12-myristate 13-acetate (PMA) (Sigma-Aldrich, MO, USA) for 24 h, and then, the media was changed to that without 1% PBS. The *H. pylori* strains, *H. pylori* 60190 (CagA+. 49503, ATCC, USA), *H. pylori* ΔCagA (CagA−), and *H. pylori* 8822(Cag PAI−), were cultured on agar plates containing 10% horse serum at 37℃ in a microaerobic atmosphere using a CampyContainer system (BBL, USA)

2.2. GC patients and tissue sampling

Patients with advanced gastric cancer (n=34) surgically removed at Yonsei University Severance Hospital and those with early gastric cancer (n=36) removed via endoscopy were selected. From each group, patients with *H. pylori* infection and those without *H.*

pylori infection were matched in a 1:1 ratio. Additionally, fresh tissues from gastric cancer and adjacent non-cancerous tissues of 66 prospectively collected patients with advanced gastric cancer were obtained from the institutional tissue bank. All samples were promptly frozen in liquid nitrogen following resection and stored at –80 °C until further use. Written informed consent was obtained from 36 early gastric cancer patients in compliance with the Declaration of Helsinki, and the study received approval from the the Public Institution Bioethics Committee designated by the Ministry of Health and Welfare and the IRB of Yonsei University College of Medicine (IRB number: 4-2013-0024; approval date: March 7, 2013). The advanced gastric cancer samples of 34 patients were obtained prior to receiving consent and were consequently exempt from consent requirements. A total of 100 samples were sourced from the Tissue Bank at the Research Institute of Gastroenterology, Yonsei University College of Medicine (Seoul, Korea). All patients had undergone gastric cancer surgery and had completed their treatment. Since the clinical data and tissue samples did not include any personal identification information, prior consent was not required. For patients with multiple tumors, tissues were taken from the largest lesions.

2.3. Total RNA extraction, reverse transcription and quantitative real-time PCR

Total RNA was extracted from GC cells and tissues using the TRIzol reagent (Invitrogen, Carlsbad, CA, USA), followed by reverse transcription and quantitative real-time PCR. RNA quantification was carried out using a Nanodrop spectrophotometer (ND-100;

Nanodrop Technologies Inc., Wilmington, DE, USA), with purity assessed through the 260/280 nm absorbance ratio and verification on 1% agarose gels. cDNA synthesis was carried out using 2.0 μg of total RNA with Superscript II (Invitrogen). The relative expression of LUCAT1 was assessed and analyzed through quantitative real-time PCR using a Light Cycler 480 Real-Time PCR machine and iQ SYBR Green Supermix (Applied Biosystems Inc., Carlsbad, CA, USA). The Ct value of the sample was normalized to the expression of *U6* or *GAPDH*, and the 2-ΔΔCt value was calculated. The primers used for qRT-PCR are presented in Table 1.

Table 1. Primer sequences for qRT-PCR

Gene	Direction	Sequence (5' to 3')
LUCAT1	Forward	5'- GCTCGGATTGCCTTAGACAG -3'
	Reverse	5'- GGGTGAGCTTCTTGTGAGGA -3'
MIF	Forward	5'- TCCGAGAAGTCAGGCACGTAG -3'
	Reverse	5'- TGCACCGCGATGTACTGG -3'
CagA	Forward	5'- TGATGAGGCAAATCAAGCAG -3'
	Reverse	5'- ATTCACGAGCTTGAGCCACT-3'
iNOS	Forward	5'- CACCATCCTGGTGGAACTCT-3'
	Reverse	5'- TCCAGGATACCTTGGACCAG-3'
IL-1β	Forward	5'- GGGCCTCAAGGAAAAGAATC-3'
	Reverse	5'- AAGTGGTAGCAGGAGGCTGA-3'
TNF-α	Forward	5'-TGGCCAATGGCGTGGAGCTG -3'
	Reverse	5'-GTAGGAGACGGCGATGCGGC-3'
Arginase-1	Forward	5'- ACTTAAAGAACAAGAGTGTGATGTG -3'
	Reverse	5'- CATGGCCAGAGATGCTTCCA -3'
IL-10	Forward	5'-AAGCCTGACCACGCTTTCTA -3'
	Reverse	5'-GCTCCCTGGTTTCTCTTCCT -3'

TGF-β	Forward	5'-GACTGCGGATCTCTGTGTCA -3'
	Reverse	5'-GGGCAAAGGAATAGTGCAGA -3'
U6	Forward	5'-CTCGCTTCGGCAGCACA-3'
	Reverse	5'-AACGCTTCAGGAATTTGCGT-3'
GAPDH	Forward	5'-CCGGGAAACTGTGGCGTGATGG-3'
	Reverse	5'-AGGTGGAGGAGTGGGTGTCGCTGTT-3'

2.4. Small interfering RNA (siRNA) transfection

For transfection, all cells are counted in 6-wells (3×10^5) and incubated in a 37 °C incubator. After 24 h, siRNA LUCAT1, MIF, and RNAi negative control (siCT; Invitrogen) were transfected according to the Lipofectamine 2000 protocol using Lipofectamine 2000 reagent (Invitrogen). The sequences of target siRNAs for LUCAT1 and MIF are listed in Table 2.

Table 2. siRNAs targeting lncRNA LUCAT1 and mRNA MIF

Gene	Direction	Sequence (5' to 3')
Si LUCAT1_1	Sense	5'- CAGAAGAUGUCAGAAGAUAAGGAUU -3'
	Antisense	5'- AAUCCUUAUCUUCUGACAUCUUCUG -3'
Si LUCAT1_2	Sense	5'- GCACAGAUAAAUUUCUCUUACUGUA -3'
	Antisense	5'- UACAGUAAGAGAAAUUUAUCUGUGC -3'
Si MIF	Sense	5'- CCGAUGUUCAUCGUAAACATT -3'
	Antisense	5'- UGUUUACGAUGAACAUCGGTT -3'

2.5. LUCAT1 overexpression plasmid construction

LUCAT1 cDNA was amplified using a PCR system (Roche Applied Science). To insert the cDNA into the pcDNA3.1 (+) expression vector, LUCAT1_NHel_F (acccaagctggctagc CAATGCCCAGACCTCCAG) and LUCAT1_Xbal_R (aaacgggccctctaga TTGACTGCAAGAGCTTGAAG) were used as cloning primers. The pcDNA3.1 (+) expression vector was purchased from Addgene. AGS and MKN74 cells were transfected with 1 μg of pcDNA3.1-LUCAT1 for 24 h using Lipofectamine 2000 (Invitrogen).

2.6. Immunofluorescence study

For the immunofluorescence study, cells were washed twice with ice-cold PBS and then incubated for 30 min at 4℃ with 4% formaldehyde in PBS. Cells were permeabilized with 0.5% Triton X-100 for 5 min, followed by blocking for 1 h in PBS containing 3% bovine serum albumin. They were then incubated with the primary antibody (CagA, sc-28368, Santa Cruz, USA; MIF, sc-271631, Santa Cruz; Alpha tubulin, sc-32293, Santa Cruz) overnight at 4 ℃. Cells were then washed multiple times with PBS containing 0.1% Tween 20, followed by incubation with anti-mouse-FITC and/or anti-rabbit-Texas Red-conjugated secondary antibody. They were then stained with DAPI for 1 h at room temperature, followed by washing with PBST. Cellular fluorescence was monitored using a Zeiss LSM 700 confocal microscope (Carl Zeiss, Germany).

2.7. ChIP-qPCR assay

For chromatin shearing was performed in lysates of cells transfected with small interfering RNA (siRNA) (siLUCAT1 or siControl), I used water bath sonication for 30 cycles under cooling conditions, 15 s, 30 s off (170–190 W). The fragmented chromatin was extracted using the High-Sensitivity ChIP Kit (ab185913; Abcam, Cambridge, UK), following the protocol provided by the manufacturer. A total of 5 μg of total chromatin was used for ChIP with anti-H3K27 acetyl (ab; Abcam) and the mock immunoprecipitation (IP) (IgG, ab185913; Abcam) at 4 ℃ overnight. After reversing cross-links and purifying the DNA, 1 μL of the eluted DNA was used for qRT-PCR with primers specific to the target regions. The sequences of the primers used for qRT-PCR are shown in Table 3.

Table 3. Primer sequences for ChIP-qPCR

Gene	Direction	Sequence (5' to 3')
Primer 1	Forward	5'- GGTGTACCCAGATGCTCCAT -3'
	Reverse	5'- CTCCGTGGTAGGCAGATGAC -3'
Primer 2	Forward	5'- AAAGAGACTGTCCCCACTGG -3'
	Reverse	5'- CCTTCAGTTCTTGGCTCAGC -3'
Primer 3	Forward	5'- CAGGGCCTTGTGACAGTACT -3'
	Reverse	5'- CATCTCCTTGTACCCTCCCC -3'
Primer 4	Forward	5'- AACTTGAGAGGGGCTTCTGG -3'
	Reverse	5'- ACCAGAGACATTCCATCCCC -3'
Primer 5	Forward	5'- GCTGGATTTAGGC GGCTTTT -3'
	Reverse	5'- GTCCCTGTGAACCTGAATG -3'
Primer 6	Forward	5'- GCTCAGCTTTCATAGGGCAC-3'
	Reverse	5'- CACCTCATCACCTGCCAGTA -3'
Primer 7	Forward	5'- GGGCACAGGTAAGAGAAGGT -3'
	Reverse	5'- TACCAGTCTCAGTGAAGGCC -3'
Primer 8	Forward	5'- AAATCTCTGAGGACCTGGCC -3'

	Reverse	5'- CACCGTGTATGGCCTCTCAT -3'
Primer 9	Forward	5'- GGAAGTTCCCTGGATGGTGA-3'
	Reverse	5'- AAGATGGCCCTTACCCTTC-3'
Primer 10	Forward	5'- TAAGAAAGACCCGAGGCGAG -3'
	Reverse	5'- GTCCCGCCTTTTGTGACG -3'

2.8. RIP Assay

To immunoprecipitate isolate RNA-protein complexes, cells were first lysed using IP buffer (Thermo Fisher Scientific) and subsequently resuspended in RIP buffer (Abcam) containing an RNase inhibitor (GenDEPOT, Barker, TX, USA) and protease inhibitor (GenDEPOT). Chromatin was sheared by sonication in a water bath for 30 cycles, followed by centrifugation to clear the lysate. An appropriate antibody (2 μg) was added to the resulting supernatant (600-800 μg) and the mixture was incubated at 4 ℃ for 24 h or more on a rotator. After incubation, 20 μL of Magna Chip protein magnetic beads (Merck Millipore) were added, and the solution was rotated at 4 ℃ for 2 h. Following washing with RIP buffer, RNA purification was performed using TRIzol reagent for qRT-PCR, and SDS gel electrophoresis was used for western blotting.

2.9. Western blot analysis

Whole cell lysates were treated with 1X RIPA buffer (Cell Signaling Technology, Danvers, MA, USA) supplemented with a protease inhibitor (GenDEPOT). Proteins were separated on sodium dodecyl sulfate-polyacrylamide gels and subsequently transferred to

polyvinylidene fluoride membranes (Millipore, Darmstadt, Germany). The membranes were then blocked at room temperature for 30 min using 3% bovine serum albumin (Thermo Fisher Scientific) before being incubated with primary antibodies. This was followed by incubation with horseradish peroxidase-conjugated goat anti-mouse and goat anti-rabbit secondary antibodies (GenDEPOT). The antibodies employed for the western blot analysis included the following: anti-CagA (CagA, sc-28368, Santa Cruz), anti-MIF (MIF, sc-271631, Santa Cruz), anti-TSG101 (TSG101, ab30871, Abcam), anti-CD63 (cd63, ab231975, Abcam), anti-HDAC1 (HDAC1, ab7028, Abcam), anti-HDAC2 (HDAC2, ab7029, Abcam), anti-Histone H3K27ac (H3K27ac, ab4729, Abcam), anti-Histone H3 (GTX115549, Genetex, Irvine, CA, USA), PTEN (PTEN, ab32199, Abcam), PI3K (PI3K, ab151549, Abcam), AKT (AKT, ab8805, Abcam), p-AKT (p-AKT, ab81283, Abcam), anti-TGF-β (TGF β, ab215715, Abcam), anti-Arginase-1 (Arginase-1, sc-166920, Santa Cruz), anti-IL-10 (IL-10, ab34843, Abcam), and anti-β-actin (β-actin, sc-47778, Santa Cruz). The membranes were subsequently treated with ECL solution (GenDEPOT) and then exposed using either an X-ray film processor (CP1000; AGFA, Greenville, SC, USA) or an Image Quant LAS 4000 (GE Healthcare, Piscataway, NJ, USA).

2.10. Exosome isolation

The medium used to culture the AGS cells was collected and centrifuged at 3000 × *g* for 10 min at 4 ◦C. The supernatant was filtered through a 0.22 μm filter (Millipore) to remove cell debris and large vesicles and ultra-centrifuged at 10,000 × *g* for 70 min at 4 ◦C. The

pellet was washed using PBS and ultra-centrifuged at 100,000 × *g* for 70 min at 4 ◦C and resuspended in PBS. The exosomes were stored at –80 ◦C until used.

2.11. Transmission electron microscopy (TEM)

For the transmission electron microscopy analysis, exosome samples were prepared as previously outlined. The exosome pellet was briefly immersed in a droplet of 2.5% glutaraldehyde in PBS buffer and left to fix overnight at 4 ℃. The exosome samples were washed three times in PBS for 10 min each, then fixed in 1% osmium tetroxide for 60 min at room temperature. Following this, the samples were dehydrated through a series of ethanol concentrations, ultimately reaching 100%. They were infiltrated with Epon resin (Ted Pella) in a 1:1 mixture of Epon and propylene oxide overnight on a rocker at room temperature. The next day the samples were placed in fresh Epon for several hours, then embedded in Epon overnight at 60 ℃. Thin sections were cut using a Leica EM UC7 ultramicrotome, collected on formvar-coated grids, stained with uranyl acetate and lead citrate, and examined using a JEOL JEM 1011 transmission electron microscope at 80 kV.

2.12. Nanoparticle tracking analysis (NTA)

The Nanosight NS 300 system (NanoSight Technology, Malvern, UK), equipped with a 488 nm laser and a high-sensitivity sCMOS camera, was used to directly monitor the number and size of exosomes. Exosomes were re-suspended in PBS at a concentration of 5 μg of protein per ml and were subsequently diluted by 100 to 500 times, aiming to achieve

a range of 20 to 100 particles visible in each frame. Samples were manually injected into the sample chamber at room temperature. Each sample was analyzed in triplicate using camera setting 13, with an acquisition time of 30 s and a detection threshold setting of 7. Each video was analyzed for a minimum of 200 completed tracks, using the NTA analytical software version 2.3 for data capture and analysis.

2.13. GW4869 treatment

GW4869, known as an inhibitor of exosome formation and release,[33] was initially dissolved in DMSO to create a 1.5 mM stock solution. To enhance solubility, 5% methanesulfonic acid was added to the DMSO. Subsequently, AGS cells were treated with GW4869 at a final concentration of 10 μM for 24 h.

2.14. Macrophage polarization

THP-1 cells were induced by PMA (160 ng/ml, 24 h; Sigma-Aldrich, Merck KGaA, Darmstadt, Germany) to differentiate into macrophages. M1 or M2 macrophages were induced by LPS (1 μg/ml, Sigma-Aldrich) + IFN-γ (50 ng/ml, R&D Systems, Minneapolis, MN, USA) or IL-4 + IL-13 (20 ng/ml, R&D Systems) for 24 h.

2.15. Flow cytometry

The expressions of non-specific macrophage marker (CD14), M1 macrophage marker (CD86) and M2 macrophage marker (CD206) were measured by a flow cytometer (EXL™,

Beckman Coulter) to determine the percentages of total macrophages ($CD14^+$), M1 macrophages ($CD14^+CD86^+$) or M2 macrophages ($CD14^+CD206^+$) in each group. PMA-induced macrophages (1×10^6) were incubated with FITC-marked CD14 antibody (ab, 10 μl, Abcam). Macrophages induced by LPS + IFN-γ were incubated with FITC-marked CD14 antibody and PerCP/Cy5.5®-marked CD86 antibody (ab, 4 μl, Abcam). Macrophages induced by IL-4 + IL-13 were incubated with FITC-marked CD14 antibody and APC-marked CD206 antibody (ab, 20 μl, Abcam).

2.16. Transwell co-culture

PMA-induced THP-1 macrophage cells (4×10^5/well) were seeded with or without each conditioned GC-derived exosomes in the upper chamber of a co-culture system with a 0.4 μm pore membrane, and the recipient AGS cells (2×10^5/well) were placed in the lower chamber. After 24 h of co-culture, AGS cells were detected and analyzed.

2.17. Cell proliferation analysis

Cell proliferation was assessed using MTS assays (Promega, Madison, WI, USA) in 96-well plates. The plates were incubated in a darkroom for 1 h, followed by enzyme-linked immunosorbent assays (ELISAs) being performed.

2.18. Colony formation assay

To assess tumorigenicity in vitro, 96-well culture plates were prepared with base and top layers of agarose using the CytoSelect™ 96-Well Cell Transformation Assay (CELL BIOLABS, INC, San Diego, CA, USA). Each well received 1.5 ml of 2X DMEM containing 1% agarose as the base layer. After 1 h solidification, AGS cells were resuspended in 2X DMEM with 0.7% agarose as the top layer and incubated at 37 ℃ for 2-3 weeks. Colonies were observed daily and images were captured using bright-field microscopy.

2.19. Invasion assay and Migration assay

For the invasion assay, AGS cells were transfected with two siLUCAT1s and subsequently reseeded in Matrigel Invasion Chambers (BD Biosciences) within a 24-well culture plate. The lower chamber was supplemented with a medium containing 10% FBS. After 24 h, the non-invading cells were carefully removed from the insert using a cotton swab. The underside of the upper chamber was fixed and stained with Diff-Quik stain (Dade Behring Inc., Newark, DE, USA). Invading cells were observed in five random fields using a virtual microscope (BX51; Olympus, Tokyo, Japan), counted, and the results were averaged.

For migration analysis, AGS cells (2×10^5) were transfected with siLUCAT1s and siCT. After 24 h of incubation, a wound was created using a P200 pipette tip. The wound width was measured at 0 and 24 h using a virtual microscope (BX51; Olympus). Image analysis was conducted using Image J software (NIH).

2.20. RNA-sequencing followed by next-generation sequencing (NGS)

RNA from AGS and GES-1 cells were treated with *H. pylori* strains 60190, 8822, and ΔCagA with 100 MOI for 6 h or transfected with CagA vector was isolated using the TRIZOL reagent (Invitrogen). For deep sequencing library preparation, we utilized the Illumina Truseq stranded and unstranded mRNA library prep kits (Illumina, USA) as per the manufacturer's instructions. The libraries were sequenced in a paired-end format to a read length of 101 bp on the HiSeq 2000 platform (Macrogen Corporation, Republic of Korea).

2.21. Statistical analysis

Data analysis was performed using Prism 5 software (GraphPad, San Diego, CA, USA). The results are shown as mean ± standard error of the mean (SEM) or as median ± interquartile range (IQR). Statistical differences between the two groups were assessed using either unpaired t-tests or Mann-Whitney tests, with a significance threshold of $P < 0.05$.

3. RESULTS

3.1. RNA-seq analysis following infecting gastric epithelial cells with H. pylori and CagA

To elucidate the role of *H. pylori* in GC cells and normal gastric epithelial cells, AGS (CC) and GES-1 cells (NC) were infected with *H. pylori* strains 60190 (C6, N6), 8822 (N6, N8), and isogenic CagA deletion mutant strain (delta CagA, ΔCagA) (C-delta, N-delta) at 100 MOI for 6 h. To further understand the role of CagA, transfection was performed using a CagA vector (CV, NV), followed by RNA-seq analysis. To assess the effect of CagA, a virulence factor representing *H. pylori* pathogenicity, in AGS cells, *H. pylori* strain 60190 (C6) and CagA transfection (CV) were compared with their respective controls: *H. pylori* strain 8822 (C8), ΔCagA (C-delta), and empty-vector transfection (CX).

RNA-seq analysis revealed that no lncRNAs exhibited significant expression changes common to all *H. pylori* strains infecting AGS and GES-1 cells (Fig. 1A–B, left). However, several lncRNAs were significantly upregulated under both CagA-positive *H. pylori* strain 60190 and CagA transfection conditions. In AGS cells, LUCAT1 (4.85- and 5.71-fold, respectively, $P < 0.05$) and ATRIP-TREX1 (read-through lncRNA) (137- and 80.9-fold, respectively, $P < 0.05$) expression was significantly upregulated by CagA-positive *H. pylori* 60190 (C6) and CagA transfection (CV) than the control (CC, CX; Fig. 1A, right). In GES-1 cells, SNHG1 (3.22- and 3.70-fold, respectively, $P < 0.05$), SNHG15 (3.74- and 5.27-fold, respectively, $P < 0.05$), ATP6V1G2-DDX39B (read-through lncRNA) (3.79- and 3.42-fold, respectively, $P < 0.05$), and CZIP-ASNS (read-through lncRNA) (5.56- and

4.57-fold, respectively, $P < 0.05$) expressions were significantly upregulated than the control (Fig. 1B, right). To validate the RNA-seq results, AGS and GES-1 cells were infected with *H. pylori* 60190, and changes in the expression of lncRNAs LUCAT1, SNHG1, and SNHG15 were examined by qRT-PCR. LUCAT1 expression significantly increased in both AGS and GES-1 cells upon infection with *H. pylori* 60190. However, only SNHG1 and SNHG15 expression changed in GES-1 cells upon infection with *H. pylori* 60190 (Fig. 1C).

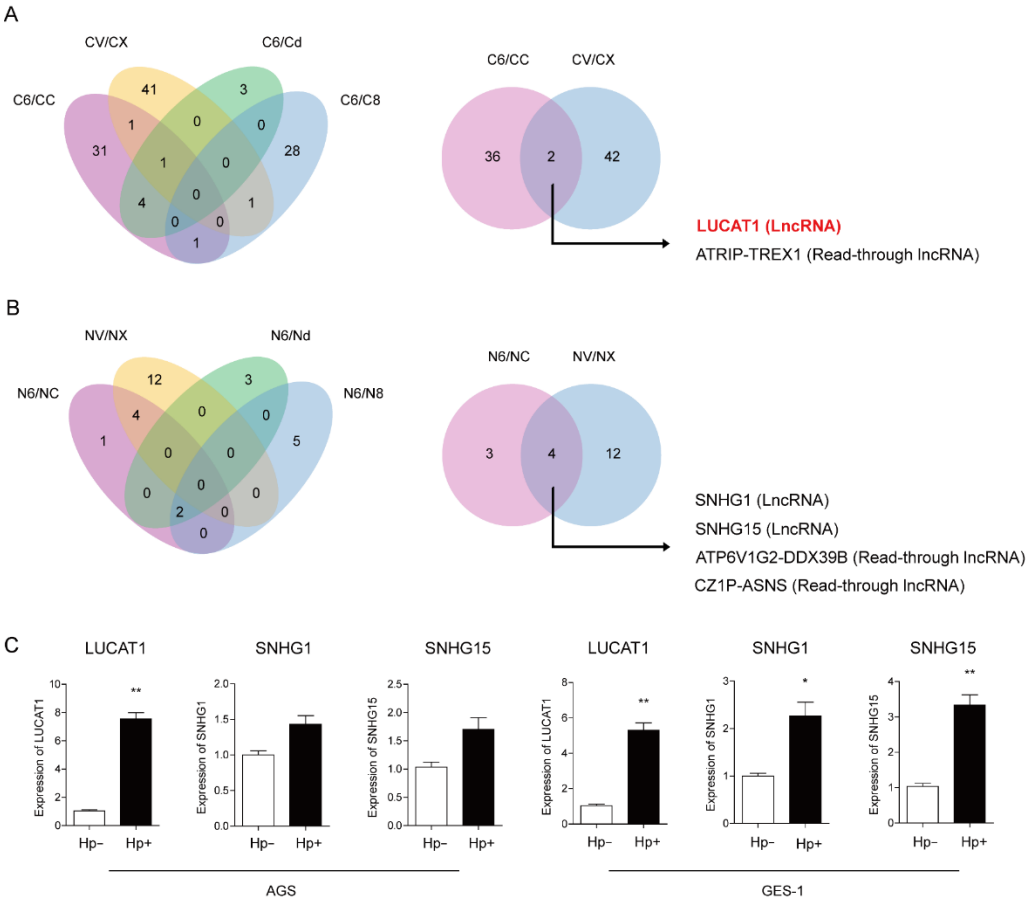

Figure 1. RNA-seq analysis following infecting gastric epithelial cells with *H. pylori* and CagA. **(A)** The Venn diagram shows overlapping lncRNAs of significantly differentially expressed lncRNAs (DELncRNAs) with [log2(FC)] > 2 and *P*-value < 0.05 following infection of each strain *H. pylori* or transfection of CagA expression vector in AGS cells (CC). **(B)** The Venn diagram shows overlapping lncRNAs of significantly differentially expressed lncRNAs (DELncRNAs) with [log2(FC)] > 2 and *P*-value < 0.05 following infection of each strain *H. pylori* or transfection of CagA expression vector in GES-1 normal gastric epithelial cells (NC). **(C)** LUCAT1, SNHG1, and SNHG15 expression after infection of CagA-positive *H. pylori* 60190 at 100 MOI for 6 h in AGS and GES-1 cells were analyzed using qRT-PCR. Hp− ; control, Hp+ ; CagA-positive *H. pylori* 60190 infection. All of the data are from three independent experiments. Data represented the mean ± s.e.m. n = 3, t test, **P* < 0.05, ***P* < 0.01, ****P* < 0.001 versus con group.

3.2 LUCAT1 exhibits a specific increase in response to infection of CagA-positive H. pylori

I validated LUCAT1 expression in 66 patients with advanced GC. LUCAT1 expression was markedly elevated in GC tissues compared to adjacent non-tumor tissues (Fig. 2A). To understand the association between LUCAT1 and GC in the context of CagA-positive *H. pylori* infection, I compared LUCAT1 and CagA expression levels in GC tissues. I examined LUCAT1 expression in 34 patients with advanced GC and 36 patients with early GC based on the presence of *H. pylori* infection and CagA. In GC tissues with *H. pylori* positivity, LUCAT1 expression was significantly higher than that in *H. pylori*-negative GC tissues (Fig. 1B–C, left). Additionally, LUCAT1 expression statistically significantly increased in CagA-positive *H. pylori*-infected GC tissues than in CagA-negative *H. pylori*-infected GC tissues (Fig. 1B–C, right).

Next, I examined LUCAT1 expression in various GC cell lines and normal gastric epithelial cells and found that its expression was significantly higher in the GC cell lines (AGS, MKN74, KATO III, and SNU719) than in normal gastric epithelial cells (GES-1) (Fig. 2D). AGS and MKN74 cell lines, which show relatively high LUCAT1 expression levels, were selected as target cells to study the mechanism of the interaction between LUCAT1 and *H. pylori*.

When AGS cells were infected with *H. pylori* 60190 at 100 MOI for 6 h, CagA expression was confirmed by western blot analysis, which showed a proportional increase with MOI (Fig. 2E, left). CagA expression initiated at 100 MOI for 3 h after infection with *H. pylori*

60190, persisted for up to 12 h, and subsequently decreased (Fig. 2E, right). LUCAT1 expression also significantly increased when infected with *H. pylori* 60190, starting at 100 MOI for 6 h (Fig. 2F, left). Moreover, LUCAT1 expression pronouncedly increased at 6 h after infection with *H. pylori* 60190 at 100 MOI (Fig. 2F, right). LUCAT1 was upregulated by infection of CagA-positive *H. pylori* 60190, and did not increase when infected with ΔCagA in AGS and MKN74 cells (Fig. 2G). This result indicates that LUCAT1 exhibits a specific response to CagA-positive *H. pylori* infection.

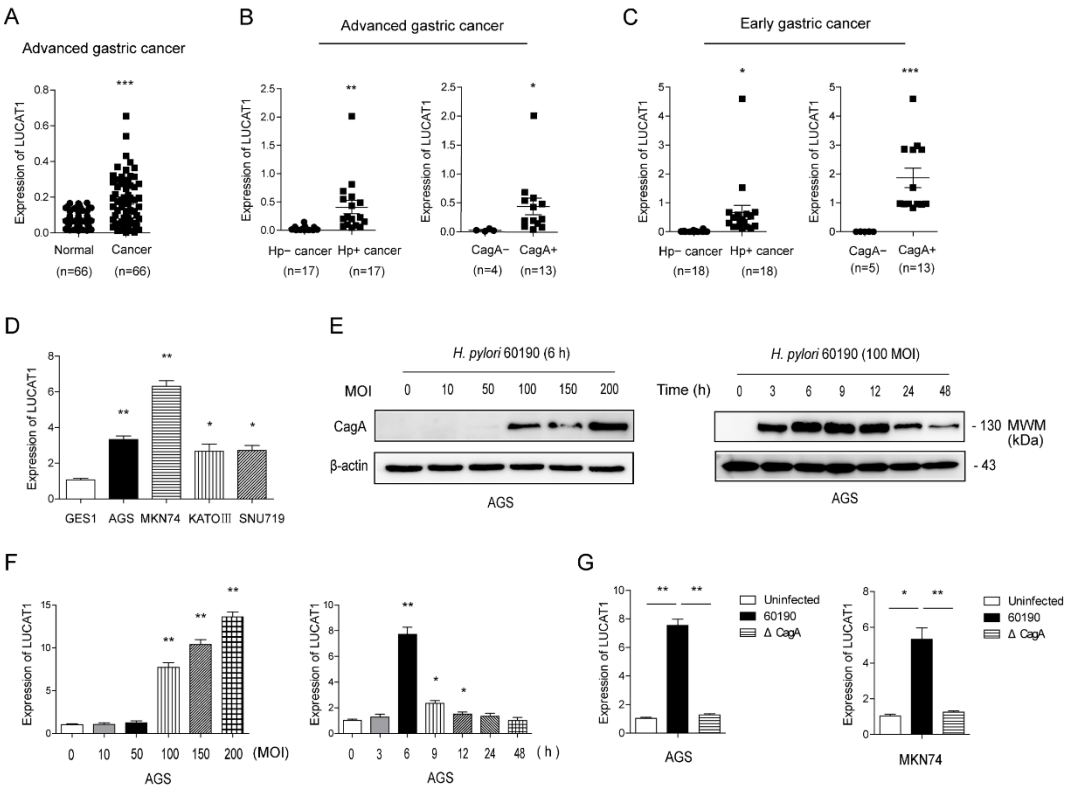

Figure 2. LUCAT1 exhibits a specific increase in response to CagA-positive *H. pylori* infection. **(A)** LUCAT1 expression in cancer tissues and adjacent non-tumor tissues (n=66) was analyzed using qRT-PCR. **(B–C)** LUCAT1 expression in advanced GC (n=34) (B) and early GC (n=36) (C) tissues

was analyzed using qRT-PCR. **(D)** LUCAT1 expression in GC cell lines (AGS, MKN74, KATO III, and SNU719) and gastric normal epithelial cells (GES-1) was analyzed using qRT-PCR. **(E)** Representative images showing CagA expression after infection of *H. pylori* 60190 at indicated dose for 6 h (left) and indicated time at 100 MOI (right) in AGS cells by western blot analysis. **(F)** LUCAT1 expression after infection of *H. pylori* 60190 at indicated dose for 6 h (left) and indicated time at 100 MOI (right) in AGS cells was analyzed by qRT-PCR. **(G)** LUCAT1 expression after infection of CagA-positive *H. pylori* 60190 or isogenic CagA deletion mutant strain (ΔCagA) at 100 MOI for 6 h in AGS and MKN74 cells was analyzed using qRT-PCR. All of the data are from three independent experiments. Data represented the mean ± s.e.m. $n = 3$, t test, $^{*}P < 0.05$, $^{**}P < 0.01$, $^{***}P < 0.001$ versus con group.

3.3 LUCAT1 acts as an upstream regulator of MIF in GC cells

I focused on the role of MIF as a key gene in illustrating the function of LUCAT1 in linking inflammatory responses to the TME in GC, which was the primary aim of this study. First, I examined the relationship between LUCAT1 and MIF expression. StarBase assay revealed that MIF and LUCAT1 expression levels were positively correlated in GC (Fig. 3A). I validated the correlation between MIF and LUCAT1 expressions in 66 patients with advanced GC (Fig. 3B). In addition, I performed a correlation analysis between MIF and LUCAT1 in 17 patients with *H. pylori*-infected advanced GC and 18 patients with *H. pylori*-infected early GC (Fig. 3C–D). I also confirmed that LUCAT1 upregulation is associated with increased MIF expression in tissue samples from both groups of patients.

Next, I examined the timing of LUCAT1 and MIF upregulation in GC cells during *H. pylori* 60190 infection at 100 MOI for 6 h in GC cells. Upon *H. pylori* 60190 infection in AGS and MKN74 cells, LUCAT1 and MIF transcription was monitored over time. LUCAT1 began to increase at 6 h post-stimulation, whereas MIF showed an increase starting from 9 h (Fig. 3E).

To determine whether there was an interaction between LUCAT1 and MIF, changes in their expression were examined after treatment with the respective siRNAs. The siRNA targeting MIF decreased both MIF transcription (Fig. 4A) and translation (Fig. 4C) in AGS and MKN74 cells but did not affect LUCAT1 expression (Fig. 4B). Two siRNAs targeting LUCAT1 (siLUCAT1_1 and siLUCAT1_2) suppressed LUCAT1 expression in AGS and MKN74 cells by approximately 50% (Fig. S1A), and decreased MIF transcription by approximately 50% (Fig. 4D). Conversely, pcDNA_LUCAT1 increased LUCAT1 expression by approximately 4000% in AGS and MKN74 cells (Fig. S1B) and upregulated MIF transcription by more than 4-fold (Fig. 4E).

Both LUCAT1 siRNAs significantly decreased MIF translation in AGS and MKN74 cells, even in the absence of *H. pylori* 60190 infection, whereas the pcDNA_LUCAT1-induced expression increased MIF translation (Fig. 4F, left). Similarly, *H. pylori* 60190 infection increased MIF translation in AGS and MKN74 cells, but siLUCAT1s suppressed this increase, whereas pcDNA_LUCAT1 further augmented MIF translation (Fig. 4F, right).

These results demonstrated that MIF expression is regulated in the same direction as LUCAT1, indicating that LUCAT1 acts as an upstream regulator of MIF.

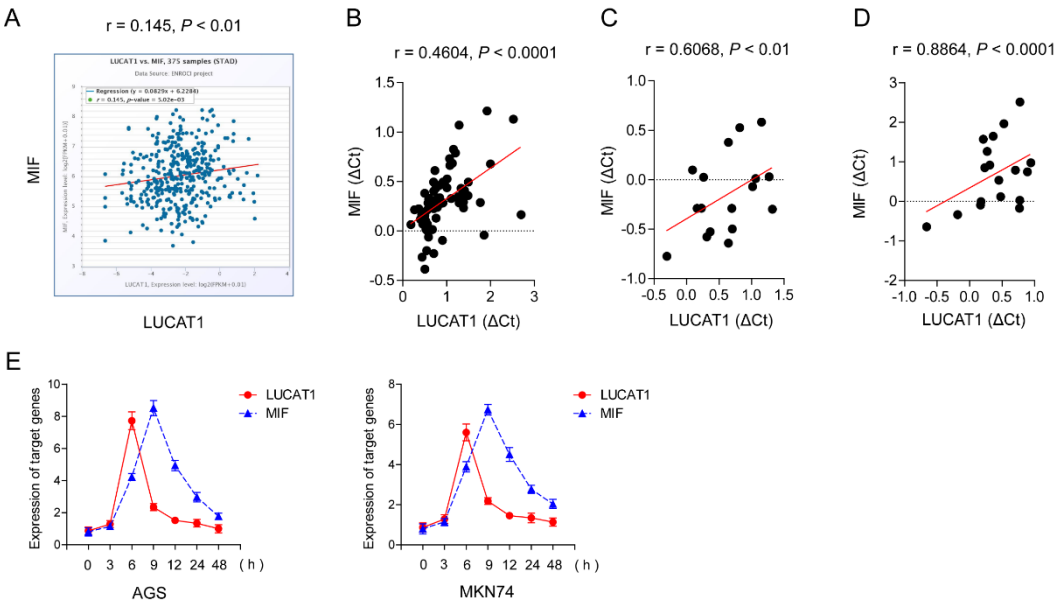

Figure 3. The expression correlation between LUCAT1 and MIF in GC tissues and cells. (A) The expression correlation between LUCAT1 and MIF in 375 cases of stomach adenocarcinoma tissues was analyzed by starBase. **(B)** The expression correlation between LUCAT1 and MIF in cancer tissues and adjacent non-tumor tissues (n=66) was analyzed using qRT-PCR. **(C–D)** The expression correlation between LUCAT1 and MIF by qRT-PCR in *H. pylori*-infected GC tissues of 17 patients with advanced GC (C) and 18 patients with early GC (D) was analyzed using Prism software; **(E)** Representative images showing the timing of LUCAT1 and MIF upregulation during *H. pylori* 60190 infection at 100 MOI for 6 h in AGS and MKN74 cells was identified by qRT-PCR.

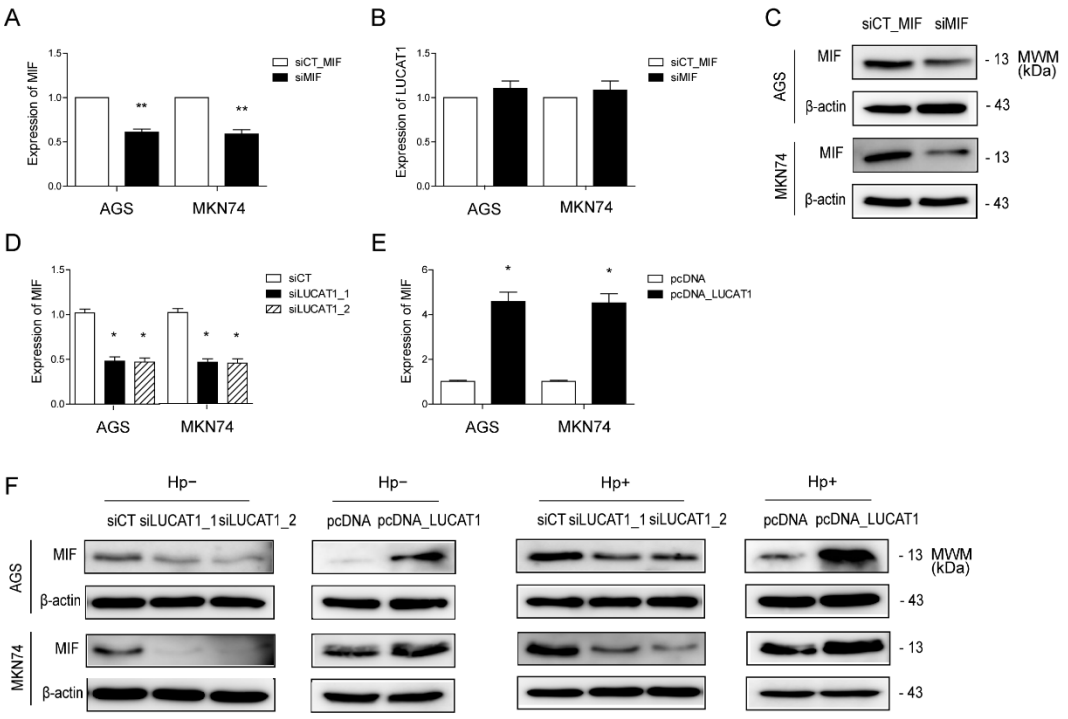

Figure 4. LUCAT1 upregulates MIF expression in GC cells. (A–B) MIF expression (A) and LUCAT1 expression (B) were measured by qRT-PCR in AGS and MKN74 cells transfected with either siControl or siMIF. **(C)** Representative images showing MIF expression in AGS and MKN74 cells transfected with either siControl or siMIF by western blot analysis. **(D)** MIF expression in AGS and MKN74 cells transfected with either siControl or siLUCAT1s was measured by qRT-PCR. **(E)** MIF expression in AGS and MKN74 cells transfected with either pcDNA or pcDNA_LUCAT1 was measured by qRT-PCR. **(F)** Representative images showing MIF expression under infection or non-infection with *H. pylori* 60190 at 100 MOI for 6 h in AGS and MKN74 cells transfected with either siControl or siLUCAT1s and either pcDNA or pcDNA_LUCAT1 by western blot analysis. All of the data are from three independent experiments. Data represented the mean ± s.e.m. $n = 3$, t test, $^{*}P < 0.05$, $^{**}P < 0.01$, $^{***}P < 0.001$ versus con group.

3.4. MIF also exhibits a specific increase in response to CagA-positive H. pylori infection

I validated MIF expression in 66 patients with advanced GC. MIF expression was significantly elevated in GC tissues compared to adjacent non-tumor tissues (Fig. 5A). To understand the association between MIF and GC in the context of CagA-positive *H. pylori* infection, I compared the MIF and CagA expression levels in GC tissues. I examined MIF expression in 34 patients with advanced GC and 36 patients with early GC based on the presence of *H. pylori* infection and CagA. In both GC tissues with *H. pylori* positivity, MIF expression was significantly increased compared to *H. pylori*-negative GC tissues (Fig. 5B–C left). Additionally, MIF expression statistically significantly increased in CagA-positive *H. pylori*-infected GC tissues than in CagA-negative *H. pylori*-infected GC tissues (Fig. 5B–C, right).

Next, I examined MIF expression in various GC cell lines and normal gastric epithelial cells and found that its expression was significantly higher in GC cell lines (AGS, MKN74, KATO III, and SNU719) than in normal gastric epithelial cells (GES-1) (Fig. 5D–E).

Furthermore, I determined the relevance of MIF to CagA. MIF was upregulated by infection of CagA-positive *H. pylori* 60190 and did not increase when infected with ΔCagA in AGS and MKN74 cells (Fig. 5F–G). After *H. pylori* 60190 infection, immunofluorescence revealed MIF and CagA accumulation in the AGS cell cytosol (Fig. 5H). These results suggest that similar to LUCAT1, MIF expression also increased by *H. pylori* 60190, with a pronounced increase specifically in response to CagA.

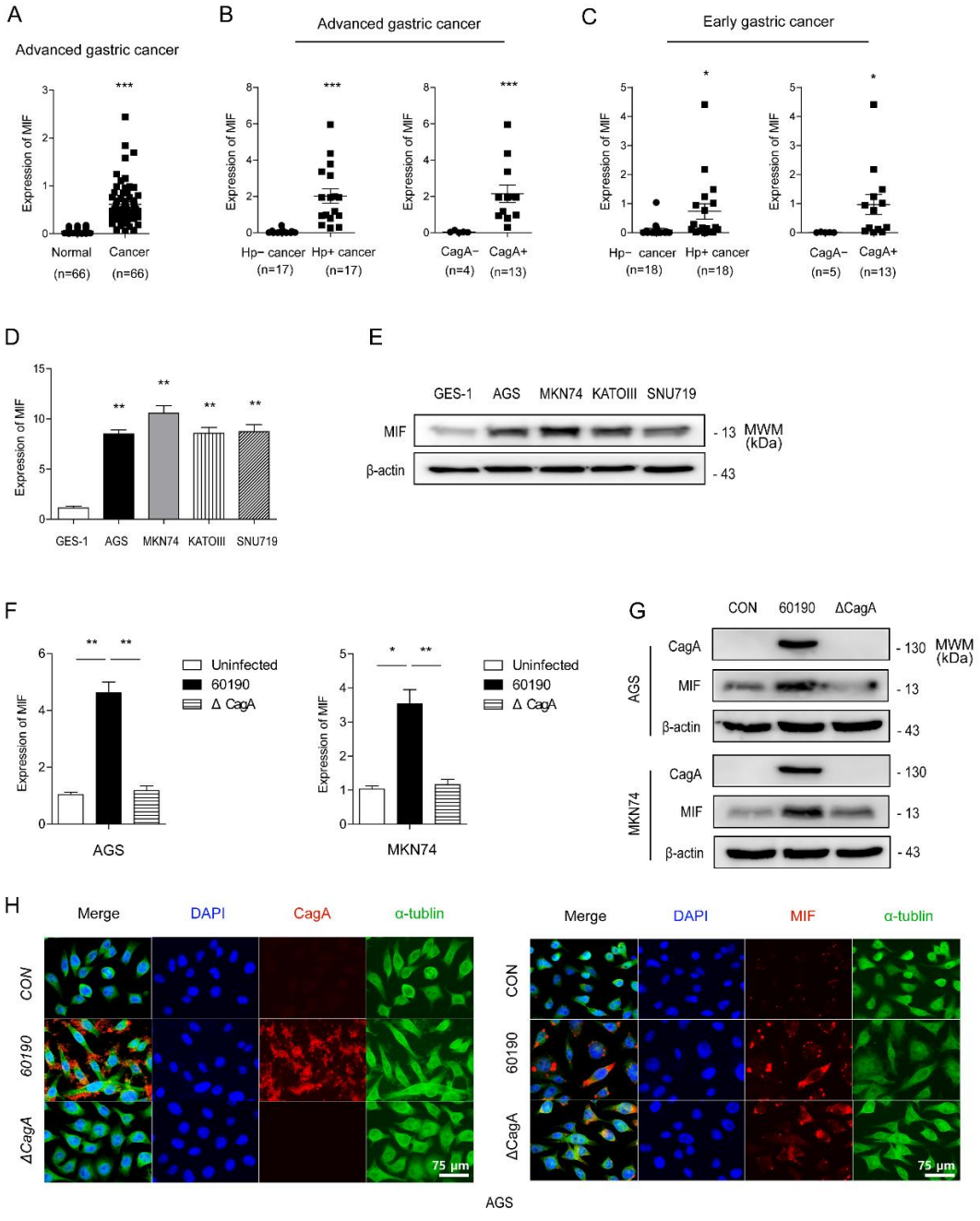

Figure 5. MIF also exhibits a specific increase in response to CagA-positive *H. pylori* infection. (A) MIF expression in cancer tissues and adjacent non-tumor tissues (n=66) was analyzed using qRT-PCR. **(B–C)** MIF expression in advanced GC (n=34) (B) and early GC (n=36) (C) tissues was analyzed using qRT-PCR. **(D–E)** MIF expression in GC cell lines (AGS, MKN74, KATO III, and SNU719) and gastric normal epithelial cells (GES-1) was analyzed using qRT-PCR (D) and western blot analysis (E). **(F–G)** MIF expression after infection of CagA-positive *H. pylori* 60190 or ΔCagA in AGS and MKN74 cells was analyzed using qRT-PCR (F) and western blot analysis (G). **(H)** Representative images showing CagA and MIF expressions with anti-CagA antibody (red), anti-MIF antibody (red), 4',6-diamidino-2-phenylindole (DAPI) nuclear stain (blue) and anti-alpha tubulin structure stain (green) after infection of *H. pylori* 60190 and ΔCagA in AGS cells by indirect immunofluorescence. All of the data are from three independent experiments. Data represented the mean ± s.e.m. $n = 3$, t test, $^{*}P < 0.05$, $^{**}P < 0.01$, $^{***}P < 0.001$ versus con group.

3.5. LUCAT1 upregulates MIF expression via H3K27 acetylation in GC cells

To investigate how LUCAT1 upregulates MIF, I examined the intracellular LUCAT1 distribution and whether this distribution changed in response to *H. pylori* infection. In both AGS and MKN74 cells, LUCAT1 was predominantly localized in the nuclear fraction compared to the control genes, *GAPDH* and *U6* (Fig. 6A). Upon *H. pylori* infection, the overall LUCAT1 expression increased in both AGS and MKN74 cells; however, the ratio of nuclear to cytosolic fractions remained unchanged (Fig. 6B).

Nucleus-localized lncRNAs have often been reported as epigenetic regulators.[34] Using UCSC, I observed a high enrichment and significant peak of H3K27 acetylation in the promoter region of MIF, suggesting that MIF is regulated by chromatin acetylation (Fig. 7A). Nevertheless, the effect of LUCAT1 on H3K27 acetylation remains unknown; therefore, Chromatin Immunoprecipitation (ChIP) was performed following LUCAT1 knockdown and *H. pylori* 60190 infection. ChIP experiments were conducted targeting

specific sequences within the MIF promoter region. Primers 7–10 each covered several CpG sites, whereas primers 1–6 did not target CpG sites. Following *H. pylori* infection, I observed an increase in acetylation, and LUCAT1 knockdown significantly decreased H3K27ac enrichment at specific sites in the MIF promoter (recognized by primers 7–10 for MIF), both before and after *H. pylori* infection (Fig. 7B). The analysis revealed that acetylated sites were evenly distributed within the CpG islands. However, sequences 500 bp away from the CpG islands showed no significant changes in acetylation. These results suggest that LUCAT1 modulates H3K27ac levels at the MIF promoter in GC cells.

Because histone acetylation is associated with histone modifications, I further investigated the interaction of LUCAT1 with well-studied histone deacetylases HDAC1 and HDAC2. I performed RIP using an HDAC1/2 antibody and found that LUCAT1 bound to HDAC1/2 (Fig. 8A–B). *H. pylori* 60190 infection increased H3K27ac levels, and while LUCAT1 knockdown reduced both baseline H3K27ac levels and the H3K27ac increase induced by *H. pylori* 60190 (Fig. 9A). However, LUCAT1 depletion did not affect HDAC1/2 expression (Fig. 9A). To investigate the interaction between MIF and HDAC1/2, I treated cells with siRNA targeting HDAC1/2. This increased the overall H3K27ac and MIF intensities (Fig. 9B). These findings suggest that LUCAT1 increase H3K27ac occupancy at the MIF promoter, thereby enhancing both baseline MIF expression and *H. pylori* 60190-induced MIF expression. This regulatory mechanism is presumed to involve the interaction with HDAC1 and HDAC2.

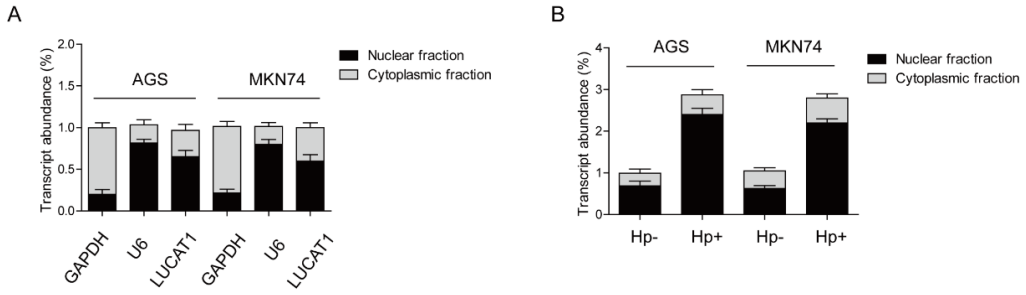

Figure 6. LUCAT1 is predominantly localized in the nuclear fraction in GC cells. (A–B) Intracellular distribution of LUCAT in AGS and MKN74 cell lysates, both uninfected (A) and infected with *H. pylori* 60190 (B), were analyzed by RT-qPCR. *GAPDH* and *U6* were used as internal control.

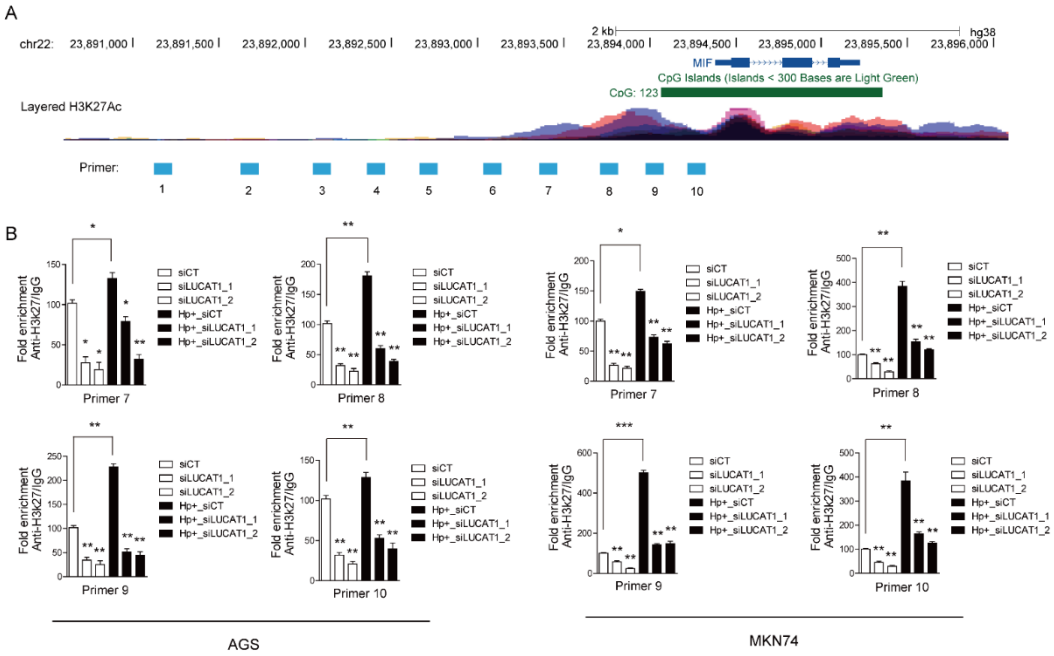

Figure 7. LUCAT1 upregulates the expression of MIF through H3K27 acetylation in GC cells. (A) Data from the UCSC Genome Bioinformatics Site (http://genome.ucsc.edu/) showed high enrichment of H3K27ac in the promoter of MIF. **(B)** ChIP-qPCR analysis of H3K27ac enrichment at MIF promoter in *H. pylori* 60190 infected or uninfected AGS and MKN74 cells transfected with either siControl or siLUCAT1s. All of the data are from three independent experiments. Data represented the mean ± s.e.m. $n = 3$, t test, $^{*}P < 0.05$, $^{**}P < 0.01$, $^{***}P < 0.001$ versus con group.

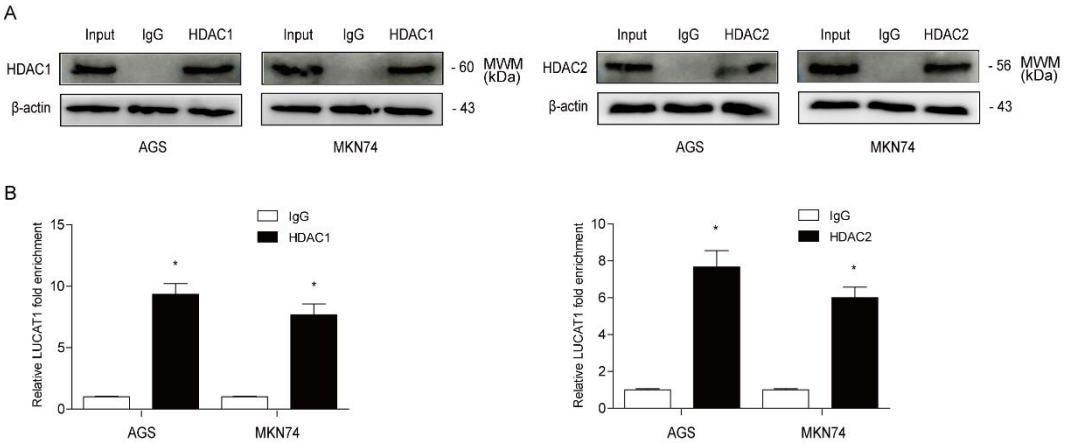

Figure 8. LUCAT1 binds with HDAC1/2. (A–B) AGS and MKN74 cells lysate was immunoprecipitated with HDAC1 and HDAC2 antibody (A) and subjected to RIP assay to detect the bindig of LUCAT1 and HDAC1/2 by qRT-PCR (B). All of the data are from three independent experiments. Data represented the mean ± s.e.m. $n = 3$, t test, $^{*}P < 0.05$, $^{**}P < 0.01$, $^{***}P < 0.001$ versus con group.

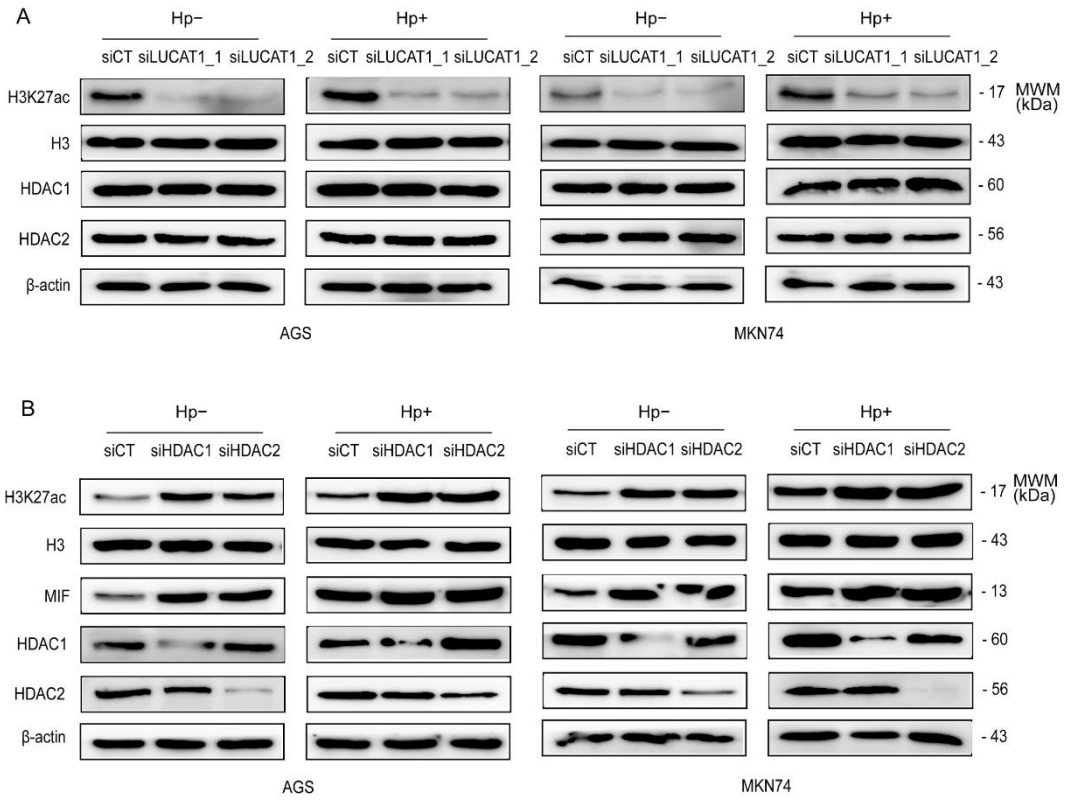

Figure 9. LUCAT1 depletion does not affect the expression of HDAC1/2. (A) Representative images showing the protein level of H3K27ac and HDAC1/2 in *H. pylor*i 60190 infected or uninfected AGS and MKN74 cells transfected with either siControl or siLUCAT1s by western blot analysis. **(B)** Representative images showing the protein level of MIF, H3K27ac, and HDAC1/2 in *H. pylori* 60190 infected or uninfected AGS and MKN74 cells transfected with either siControl or siHDAC1/2 by western blot analysis.

3.6. H. pylori-infected GC cell-derived exosomal MIF promotes macrophage toward the M2 phenotype through the PTEN/PI3K/AKT pathway

After confirming that *H. pylori* infection increased MIF expression through LUCAT1 regulation, I investigated the role of MIF in *H. pylori* infection in the context of the TME. MIF plays a critical role in inflammation and cancer progression by influencing surrounding immune cells via exosomes.[35-38]

I first confirmed the presence of exosomes in AGS cells. AGS cells were infected with *H. pylori* 60190 and transfected with siControl or siLUCAT1s to detect the presence of exosomes. Each exosome group (Hp−_Exo, Hp+_Exo, Hp+_siLUCAT1_Exo, and Hp+_siLUCAT1_2_Exo) was extracted and purified from AGS cell supernatant by differential centrifugation, which were subsequently characterized by transmission electron microscopy (TEM), nanosight tracking analysis (NTA), and western blotting. TEM images and NTA showed that the AGS cell-derived exosomes were round particles (Fig. 10A) approximately 100 nm in diameter (Fig. 10B). Western blot analysis confirmed that MIF and the exosome markers TSG101 and CD63 were detected in exosomes infected with or without *H. pylori* 60190 in siControl- or siLUCAT1-transfected AGS cells, which diminished after GW4869 treatment and inhibited neuraminidase activity in cells, thereby inhibiting tumor cell exosome secretion (Fig. 10C). These data imply that MIF can be encapsulated and secreted in GC cell-derived exosomes; exosomal MIF expression significantly increased with the expression in *H. pylori*-infected GC cells and was downregulated in siLUCAT1-transfected cells. These results suggest that *H. pylori* 60160

not only increases MIF levels in GC but also elevates exosomal MIF in GC, which is attenuated by LUCAT1 knockdown. This process may be attributed to the generation and secretion of exosomes, involving GW4869.

To understand the role of *H. pylori*-infected GC cell-derived exosomes in macrophage polarization, I first induced human THP-1 monocytes into macrophages with 160 ng/mL PMA for 24 h, and then treated them with 50 ng/mL IFN-γ and 1 μg/mL LPS to polarize into M1 macrophages or 20 ng/mL IL-4 + IL-13 to polarize into M2 macrophages for 24 h (Fig. 11A). To explore the effect of *H. pylori*-infected GC cell-derived exosomes on the macrophages in the TME, I incubated PMA-induced THP cells (M0 macrophages) with PBS, Hp−_Exo, Hp+_Exo, Hp+_siLUCAT1_1_Exo, or Hp+_siLUCAT1_2_Exo. I measured the M1 and M2 macrophage-associated phenotypic marker levels in the different groups by qRT–PCR. The M2 marker (Arginase-1, IL-10, and TGF-β) levels in macrophages incubated with GC cell-derived exosomes, particularly *H. pylori*-infected GC cell-derived exosomes, were significantly increased, while those of M1 markers (iNOS, IL-1β, and TNF-α) were not significantly different. Incubation with Hp+_siLUCAT1s_Exo, which depletes exosomal MIF expression, attenuated these effects (an increase in M2 markers) (Fig. 12A). According to the measurement of the expression of the surface markers CD14 (all macrophages), CD206 (M2 macrophages), and CD86 (M1 macrophages) by flow cytometry, the proportion of $CD14^+CD86^+$ macrophages in each group did not change significantly after treatment with GC cell-derived exosomes (Fig. 13A, above). $CD14^+CD206^+$ macrophages reduced in the Hp+_siLUCAT1s_Exo group and increased in

the Hp+_Exo group (Fig. 13A, below).

I explored the mechanisms underlying M2 macrophage polarization induction by *H. pylori*-infected GC cell-derived exosomal MIF. The PTEN/PI3K/AKT signaling pathway is involved in macrophage polarization.[39-41] Therefore, I hypothesized that *H. pylori*-infected GC cell-derived exosomal MIF promotes M2 macrophage polarization via the PTEN/PI3K/AKT signaling pathway. To test my hypothesis, I performed a series of western blotting analyses and found that *H. pylori*-infected GC cell-derived exosomal MIF activated the PTEN/PI3K/AKT signaling pathway. Hp+_Exo incubated group downregulated PTEN expression and upregulated PI3K, p-AKT, and M2 marker (TGF-β, Arginase-1, and IL-10) expressions; Hp+_siLUCAT1s_Exo, which is thought to deplete exosomal MIF expression, attenuated the above effects (Fig. 14A). Collectively, these results suggest that *H. pylori*-infected GC cell-derived exosomal MIF activates the PI3K/p-AKT/AKT signaling pathway to induce macrophage M2 polarization by downregulating PTEN expression in macrophages.

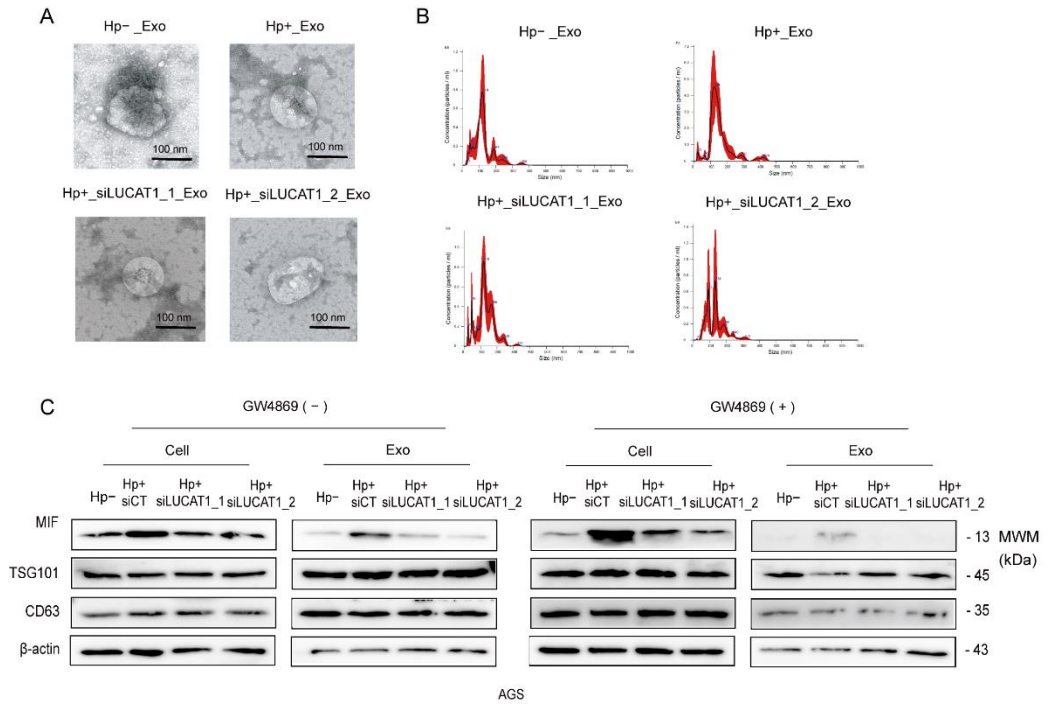

Figure 10. Identification of GC cell-derived exosomes and GW4869 decreases the secretion of GC cell-derived exosomes. (A) Representative TEM images of GC cell (AGS) derived exosomes. (scale bar = 100 nm) **(B)** Exosome size distribution as analyzed by NTA. **(C)** Representative images showing exosomal MIF and exosomal surface markers TSG101 and CD63 expression in AGS cells treated with or without 10 μM GW4869 for 24 h, an inhibitor of exosome secretion, by western blot analysis.

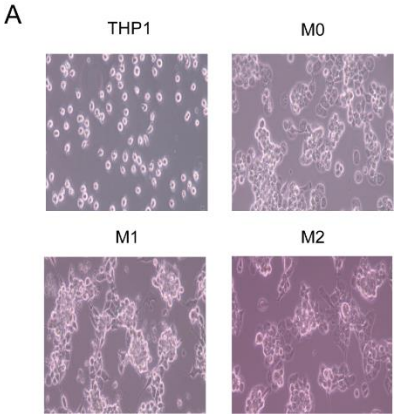

Figure 11. Identification of PMA-mediated differentiation of THP-1 macrophages. (A) Representative images showing PMA-mediated differentiation of THP-1 macrophages by microscopy.

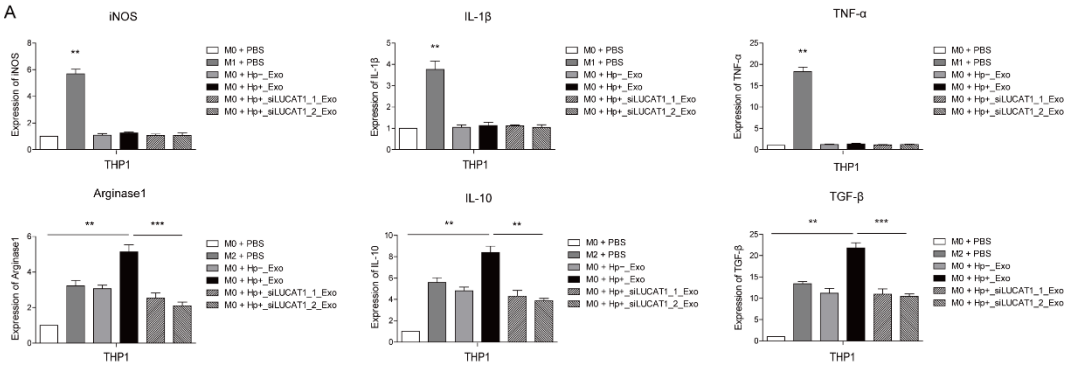

Figure 12. *H. pylori*-infected GC cell-derived exosomes induce macrophages to differentiate into M2 macrophages. (A) The expression of M1 markers (iNOS, IL-1β, and TNF-α) and M2 markers (Arginase-1, IL-10, and TGF-β) in THP-1 macrophages incubated with or without each group of GC cell-derived exosomes was analyzed by qRT-PCR. All of the data are from three independent experiments. Data represented the mean ± s.e.m. n = 3, t test, $*P < 0.05$, $**P < 0.01$, $***P < 0.001$ versus con group.

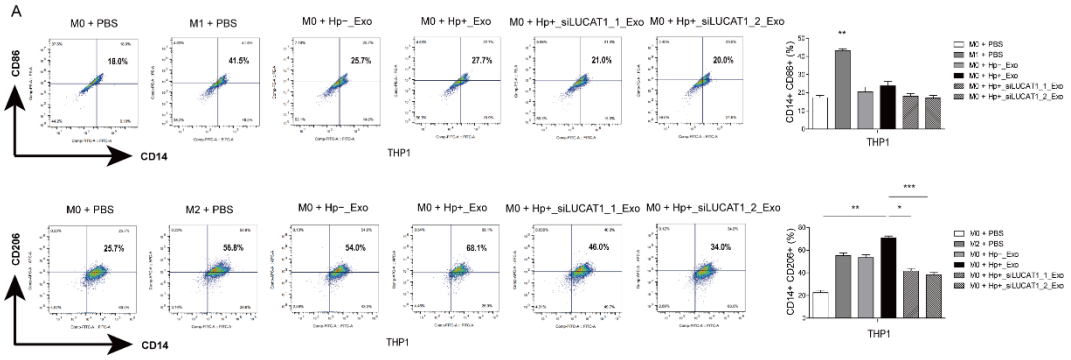

Figure 13. Flow cytometry showing regions of M2 macrophage ($CD14^+$ $CD206^+$) induced by *H. pylori*-infected GC cell-derived exosomes. (A) Representative images showing macrophage marker (CD14), M1 macrophage-related phenotypic marker (CD86) and M2 macrophage-related phenotypic marker (CD206) on the surfaces in THP-1 macrophages incubated with or without each group of GC cell-derived exosomes by flow cytometry. Flow cytometry dot plot showing regions of considered M1 macrophage ($CD14^+$ $CD86^+$) and M2 macrophage ($CD14^+$ $CD206^+$) with indicated percentages, was measured in THP-1 macrophages gated on live cells. All of the data are from three independent experiments. Data represented the mean ± s.e.m. n = 3, t test, $*P < 0.05$, $**P < 0.01$, $***P < 0.001$ versus con group.

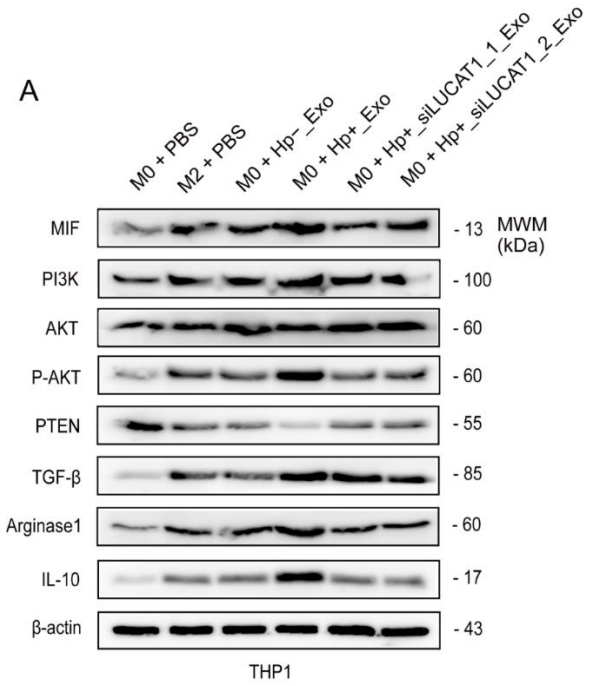

Figure 14. *H. pylori*-infected GC cell-derived exosomal MIF promotes macrophage toward the M2 phenotype through the PTEN/PI3K/AKT pathway. (A) Representative images showing MIF, PI3K, AKT, p-AKT, PTEN and M2 markers (TGF-β, Arginase-1, and IL-10) expression in THP-1 macrophages incubated with or without each group of GC cell-derived exosomes by western blot analysis.

3.7. H. pylori-infected GC cell-derived exosomal MIF induces M2 macrophage polarization to promote the GC cell proliferation and metastasis

Several studies have reported that tumor-derived exosome-induced M2 macrophage polarization promotes GC metastasis.[42-44] Therefore, I studied the role of *H. pylori*-infected GC cell-derived exosome-induced M2 macrophages in GC cell proliferation and

metastasis using an *in vitro* indirect co-culture system (Fig. 15A). The in vitro indirect co-culture system was established by isolating *H. pylori*-infected GC-derived exosomal MIF and incorporating it into the culture medium of THP-1 macrophages for 24 h incubation. As illustrated in Figure 15A, a dual-chamber setup was employed, wherein THP-1 macrophages in the upper chamber were co-cultured with AGS cells in the lower chamber for additional 24 h prior to subsequent experimental analyses. Proliferation (Fig. 16A), colony formation (Fig. 16B), invasion (Fig. 17A), and migration (Fig. 17B) levels of AGS cells co-cultured with THP-1 macrophages incubated with Hp+_Exo were higher than of those incubated with Hp−_Exo. These levels were attenuated in AGS cells co-cultured with THP-1 macrophages incubated with Hp+_siLUCAT1s_Exo, which deplete exosomal MIF expression. Collectively, these data suggest that M2 macrophages activated by *H. pylori* 60190-infected GC cell-derived exosomal MIF promote cell proliferation, colony formation, and metastasis in GC. Reducing exosomal MIF by knocking down LUCAT1 effectively modulates macrophage polarization in the TME, thereby impeding the progression of GC.

In this study, I demonstrate that CagA-positive *H. pylori* enhances MIF production and exosomal excretion in GC cells through LUCAT1 activation. The exosomal MIF induces M2 macrophages in the surrounding microenvironment, contributing to the progression of GC (Fig. 18A).

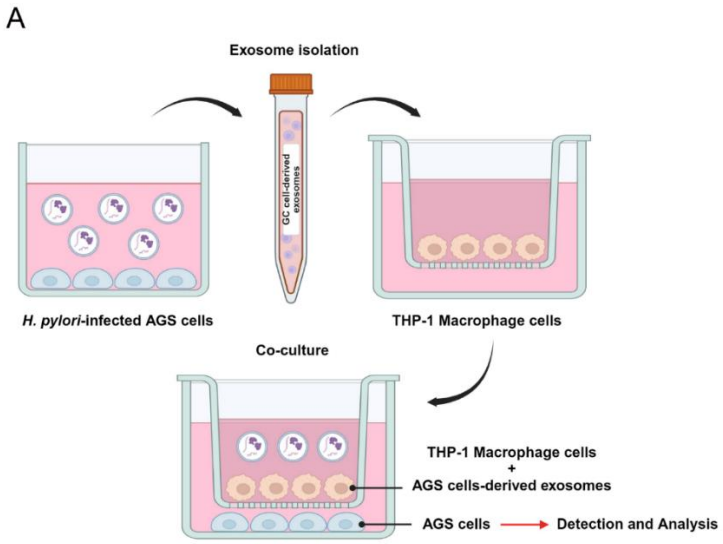

Figure 15. Co-culture between THP-1 macrophages incubated with GC cell-derived exosomes and AGS cells. (A) AGS cells were co-cultured with THP-1 macrophages incubated with or without each group of GC cell-derived exosomes in a co-culture chamber to avoid direct cell contact.

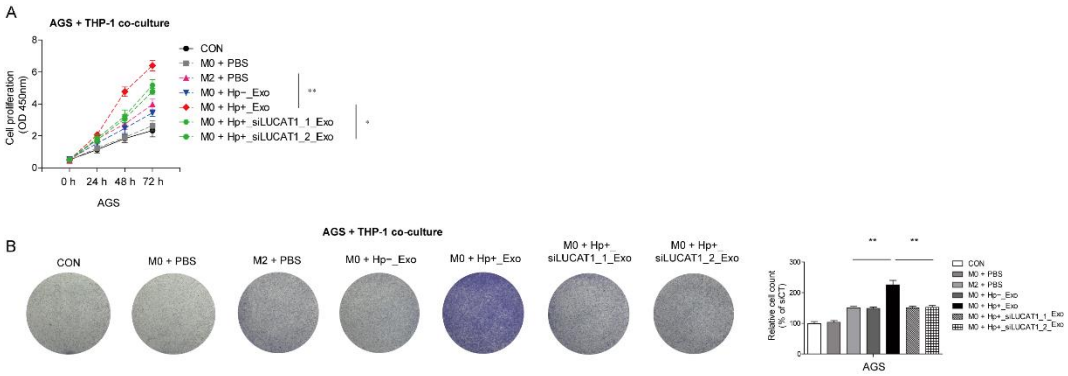

Figure 16. *H. pylori*-infected GC cell-derived exosomal MIF induces M2 macrophage polarization to promote the GC cell proliferation and colony formation. (A) MTS assays were performed to determine cell viability at 0, 24, 48, 72 h with or without each group of GC cell-derived exosomes. **(B)** Representative images showing clone formation ability in AGS cells co-cultured with THP-1 macrophages incubated with or without each group of GC cell-derived exosomes by colony formation assays. All of the data are from three independent experiments. Data represented the mean ± s.e.m. $n = 3$, t test, $^{*}P < 0.05$, $^{**}P < 0.01$, $^{***}P < 0.001$ versus con group.

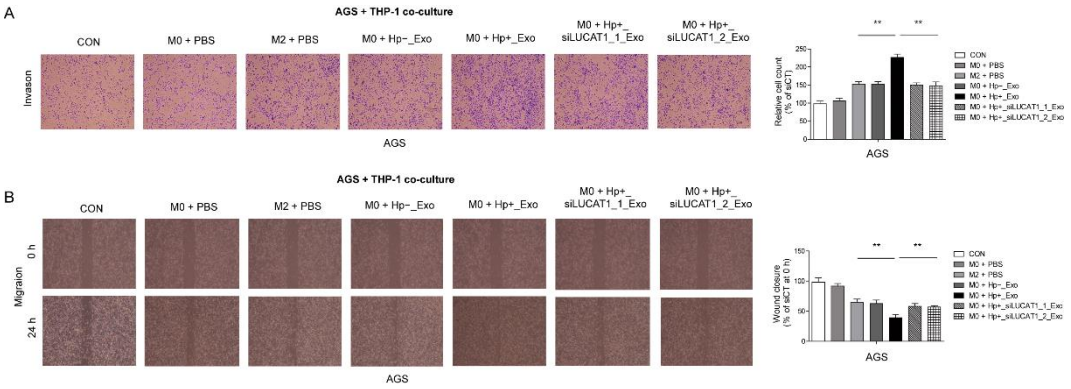

Figure 17. *H. pylori*-infected GC cell-derived exosomal MIF induces M2 macrophage polarization to promote the GC cell invasion and migration. (A) Representative images showing AGS cells co-cultured with THP-1 macrophages incubated with or without each group of GC cell-derived exosomes by invasion assays via transwell assay. **(B)** Representative images showing AGS cells co-cultured with THP-1 macrophages incubated with or without each group of GC cell-derived exosomes by migration assays via wound healing assay. All of the data are from three independent experiments. Data represented the mean ± s.e.m. $n = 3$, t test, $^{*}P < 0.05$, $^{**}P < 0.01$, $^{***}P < 0.001$ versus con group.

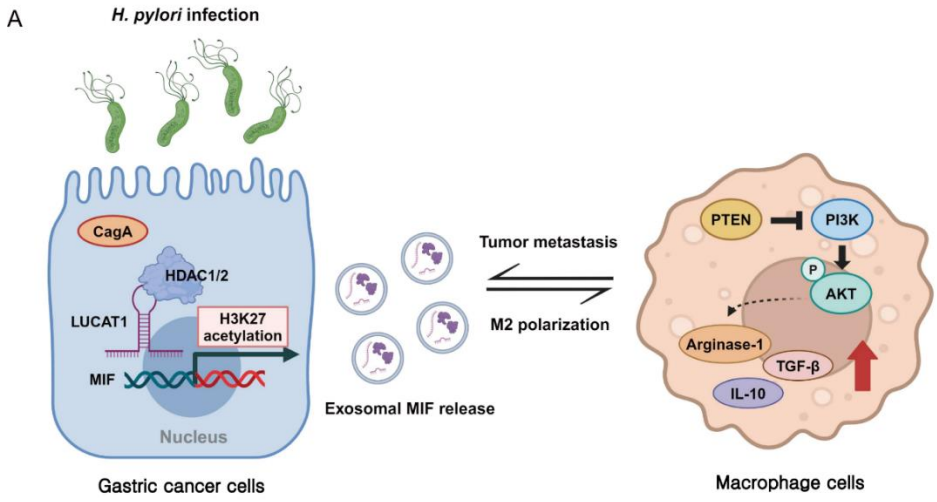

Figure 18. (A) Schematic mechanism showing how LUCAT1 induced by CagA-positive *H. pylori 60190* promotes GC metastasis by modulating M2 macrophage polarization via exosomal MIF/PTEN/PI3K/AKT pathway.

4. DISCUSSION

Despite the experimental and clinical evidence that *H. pylori* induces GC[1] and large-scale clinical studies showing that eradicating *H. pylori* reduces the incidence of GC[45], research is still ongoing to determine the precise mechanisms of GC development and progression. Such research is essential for devising more refined methods of GC prevention that could reduce the risks and inconveniences associated with *H. pylori* eradication therapy, which relies on antibiotics. In my study, through RNA sequencing and subsequent validation, I successfully identified CagA-induced LUCAT1 and MIF expression. In this study, I found that *H. pylori*, through a process not yet fully understood, induces changes in the TME by shifting macrophages from the M1 to the M2 phenotype. This process is initiated by LUCAT1 upregulation in the mucosal and GC cells by *H. pylori*, which facilitates the exosomal transfer of MIF to the TME. The exosomal MIF-induced M2 polarization of macrophages contributes to an aggressive GC phenotype, highlighting the importance of lncRNA-mediated mechanisms in GC progression. These findings suggest the potential for developing preventive and therapeutic strategies for GC by targeting LUCAT1 and MIF.

LncRNAs have diverse roles and functions in both physiological and pathological contexts, and numerous studies have demonstrated that most noncoding RNAs exert their biological effects by regulating gene expression.[22,46] The dysregulation of lncRNAs plays a pivotal role in cancer development and is closely associated with the progression of

various cancers, including gastric, colon, and lung cancers.[23,47] Consequently, lncRNAs have emerged as potential biomarkers for cancer diagnosis.[48]

With the emergence of high-throughput technologies like RNA-seq, the identification and characterization of lncRNAs have been significantly improved, leading to the development of various pipelines for identifying novel lncRNAs from RNA-seq data.[49,50] Despite successful research demonstrating the crucial roles of lncRNAs in various diseases, there is still limited understanding of their functions in GC. Moreover, elucidating the biological roles of lncRNAs remains challenging due to their limited annotations and generally low expression levels.

In this study, I elucidated the role of lncRNAs in *H. pylori*-associated GC and performed RNA-Seq to explore the lncRNA expression patterns in *H. pylori*-infected GES-1 and AGS cells, revealing a full-scale lncRNA map of *H. pylori*-infected epithelial cells. I found that LUCAT1 was upregulated in CagA-positive *H. pylori*-infected GC cells and found at higher levels in *H. pylori*-infected GC tissues than in *H. pylori*-uninfected GC tissues, with particularly elevated levels in patients with GC infected with CagA-positive *H. pylori*. I also found that the CagA-positive *H. pylori* strain 60190 induced a more pronounced elevation in LUCAT1 expression than the ΔCagA strain. These results suggest a strong correlation between LUCAT1 upregulation and the presence of CagA during *H. pylori* infection.

I have previously shown that LUCAT1 was extensively expressed in GC tissues than in adjacent non-tumor tissues and downregulated tumor suppressor genes.[26] In this study, I

reaffirmed that LUCAT1 is highly expressed in GC tissues. I identified that LUCAT1, which is upregulated by *H. pylori*, influences the TME by facilitating macrophage transition from the M0 to M2 phenotype, thereby promoting GC development. Additionally, these findings indicate that exosomal MIF secretion is integral to this mechanism. MIF, a pro-inflammatory cytokine, has been implicated in the progression of various tumors including melanoma, neuroblastoma, myelomonocytic leukemia, prostatic cancers of the breast, colon, lung, liver, stomach, and esophagus, implying its role in carcinogenesis.[19] Previous studies have shown that *H. pylori* infection increases MIF expression in both gastric inflammatory and epithelial cells, leading to the hypothesis that *H. pylori* contributes to GC development via an MIF-mediated pathway.[51]

LUCAT1 knockdown was reported to reduce HDAC1 expression in papillary thyroid cancer[52]; however, the relationship between LUCAT1 and HDAC1 or HDAC2 in other cancers has not been documented. In my study, LUCAT1 upregulates MIF expression through epigenetic modifications, particularly by modulating H3K27 acetylation at the MIF promoter via binding to HDAC1/2. This mechanism is similar to previously reported mechanisms involving MIF expression through H3K27 acetylation in astrocytes.[53] This implies that the CagA-positive *H. pylori* infection-driven LUCAT1 overexpression likely acts primarily within the nucleus and may contribute significantly to the pathogenic processes associated with *H. pylori*-related GC. Histone acetylation is a post-translational modification that plays a key role in modulating chromatin structure and transcriptional activity. Histone acetylation neutralizes the positive charge of lysine residues, leading to

chromatin decondensation and reduced interactions between DNA and histones, facilitating increased transcriptional activity.[54] Bioinformatic analysis using genome databases (http://genome.ucsc.edu/) indicated significant H3K27ac enrichment in the MIF promoter region. I confirmed the presence of H3K27ac at the MIF promoter in AGS and MKN74 cells using ChIP assays. Subcellular fractionation studies have shown that LUCAT1 is predominantly localized in the nucleus, suggesting its potential role in transcriptional regulation.

In this study, I confirmed that LUCAT1 knockdown significantly reduced H3K27ac levels in the MIF promoter, and identified LUCAT1 as a key regulator of MIF expression in GC cells. Similar to previous reports indicating that the lncRNA ANRIL regulates histone modifications through the formation of a complex with WDR5 and HDAC3 in vascular smooth muscle cells[55], LUCAT1 binds to HDAC1/2 in this study. In this study, LUCAT1 suppression alone changed H3K27ac levels at the MIF promoter compared to those achieved by siRNA targeting HDAC1/2, suggesting that LUCAT1 exerts a significant regulatory influence on MIF expression.

Tumor cells advance malignant tumor progression by secreting exosomes that mediate paracrine or endocrine signaling to mononuclear macrophages, both locally and distantly[38]. These exosomes facilitate macrophage polarization toward the M2 phenotype and elevate the levels of inflammatory factors that promote tumor progression and EMT[15]. Tumor cells can induce macrophage polarization toward the M2 phenotype, which subsequently facilitates tumor growth and progression[56]. In hepatocellular carcinoma, M2 macrophages

effectively promote malignant transformation and tumor progression compared to M1 macrophages through the upregulation of key factors such as vascular endothelial growth factor A (VEGF-A) and matrix metalloproteinase-9 (MMP-9) within the TME, contributing to poor prognostic outcomes.[57]

In this study, *H. pylori*-infected GC cell-derived exosomes were incubated with macrophages. In my study, the delivered exosomes induced M2 macrophage polarization. This effect is mediated by MIF, which is upregulated by LUCAT1 in response to CagA-positive *H. pylori* infection in GC cells. I confirmed that the secreted MIF was efficiently transferred to macrophages via exosomes and facilitated M2 polarization through the PTEN/PI3K/AKT pathway. Furthermore, M2-polarized macrophages significantly enhance GC cell proliferation, colony formation, migration, and invasion in vitro. These findings underscore the essential role of exosomal MIF, which is upregulated by *H. pylori*-CagA induced LUCAT1, in the TME acting as a crucial intercellular communication mediator and influencing tumor dynamics.

My study has several limitations that warrant further attention. Unlike my study, previous studies have reported several lncRNAs induced by *H. pylori* infection, including H19, LINC00152, and AF147447.[58-60] One potential reason for these differences may be due to the experimental design, which used both GC and normal cells. By treating these cells with various strains and toxins, I aimed to identify the lncRNAs that exhibited common expression anomalies across all conditions. This approach may have contributed significantly to the observed variations. Moreover, differences may arise from the specific

H. pylori strains used or the activity levels of the CagA vector. Nevertheless, I believe that my study provides more meaningful results than other studies, owing to its consideration of a broad range of cell types, strains, and toxins. Second, while my research confirmed that LUCAT1 increases exosomal MIF expression and enhances both MIF production and delivery in GC cells, I could not determine which of these mechanisms was the predominant pathway. However, further studies are required to address this issue.

This study provides novel perspectives on the role of lncRNA LUCAT1 and exosomal MIF in *H. pylori*-induced GC, highlighting their potential for preventive and therapeutic interventions. Future studies should explore the therapeutic efficacy of disrupting these pathways and their potential to improve outcomes in patients with GC.

5. CONCLUSION

This study provides novel perspectives on the role of lncRNA LUCAT1 in the context of *H. pylori*-induced GC. The upregulation of LUCAT1 in CagA-positive *H. pylori*-infected GC cells led to increased production of MIF, which was then secreted into exosomes. These exosomes facilitated the transfer of MIF to tumor-associated macrophages, promoting their M2 polarization and enhancing the metastatic potential of GC cells. The findings demonstrate that *H. pylori* infection significantly impacts the tumor microenvironment by modulating lncRNA expression and exosome-mediated communication. The M2 polarization of macrophages induced by exosomal MIF contributed to a more aggressive cancer phenotype, highlighting the importance of lncRNA-mediated mechanisms in GC progression.

This research underscores the potential for targeting lncRNAs and exosomal factors as therapeutic strategies in managing *H. pylori*-associated GC. Future studies should further explore the therapeutic efficacy of disrupting these pathways and their potential in improving patient outcomes in GC.

References

1. Amieva M, Peek Jr RM. Pathobiology of Helicobacter pylori–induced gastric cancer. Gastroenterology 2016;150:64-78.
2. Kwok T, Zabler D, Urman S, Rohde M, Hartig R, Wessler S, et al. Helicobacter exploits integrin for type IV secretion and kinase activation. Nature 2007;449:862-6.
3. Segal E, Cha J, Lo J, Falkow S, Tompkins L. Altered states: involvement of phosphorylated CagA in the induction of host cellular growth changes by Helicobacter pylori. Proc Natl Acad Sci U S A 1999;96:14559-64.
4. Asahi M, Azuma T, Ito S, Ito Y, Suto H, Nagai Y, et al. Helicobacter pylori CagA protein can be tyrosine phosphorylated in gastric epithelial cells. J Exp Med 2000;191:593-602.
5. Zhao Y, Zhang J, Cheng AS, Yu J, To KF, Kang W. Gastric cancer: genome damaged by bugs. Oncogene 2020;39:3427-42.
6. Polakovicova I, Jerez S, Wichmann IA, Sandoval-Bórquez A, Carrasco-Véliz N, Corvalán AH. Role of microRNAs and exosomes in Helicobacter pylori and Epstein-Barr virus associated gastric cancers. Front Microbiol 2018;9:636.
7. Jia W, Zhang J, Ma F, Hao S, Li X, Guo R, et al. Long noncoding RNA THAP9-AS1 is induced by Helicobacter pylori and promotes cell growth and migration of gastric cancer. Onco Targets Ther 2019:6653-63.
8. Zhu H, Wang Q, Yao Y, Fang J, Sun F, Ni Y, et al. Microarray analysis of Long non-coding RNA expression profiles in human gastric cells and tissues with Helicobacter pylori Infection. BMC Med Genomics 2015;8:1-11.
9. Fiocca R, Luinetti O, Villani L, Chiaravalli A, Capella C, Solcia E. Epithelial cytotoxicity, immune responses, and inflammatory components of Helicobacter pylori gastritis. Scand J Gastroenterol 1994;29:11-21.
10. Bergin PJ, Anders E, Sicheng W, Erik J, Jennie A, Hans L, et al. Increased production of matrix metalloproteinases in Helicobacter pylori-associated human gastritis. Helicobacter 2004;9:201-10.
11. Whitney AE, Emory TS, Marty AM, O'shea PA, Newman GW, Gold BD. Increased macrophage infiltration of gastric mucosa in Helicobacter pylori-infected children. Dig Dis Sci 2000;45:1337-42.
12. Mosser DM, Edwards JP. Exploring the full spectrum of macrophage activation. Nat Rev

Immunol 2008;8:958-69.

13. Gordon S, Martinez FO. Alternative activation of macrophages: mechanism and functions. Immunity 2010;32:593-604.
14. Murray PJ. Macrophage polarization. Annu Rev Physiol 2017;79:541-66.
15. Guo W, Li Y, Pang W, Shen H. Exosomes: a potential therapeutic tool targeting communications between tumor cells and macrophages. Mol Ther 2020;28:1953-64.
16. Colombo M, Raposo G, Théry C. Biogenesis, secretion, and intercellular interactions of exosomes and other extracellular vesicles. Annu Rev Cell Dev Biol 2014;30:255-89.
17. Valadi H, Ekström K, Bossios A, Sjöstrand M, Lee JJ, Lötvall JO. Exosome-mediated transfer of mRNAs and microRNAs is a novel mechanism of genetic exchange between cells. Nat Cell Biol 2007;9:654-9.
18. Hosseini R, Sarvnaz H, Arabpour M, Ramshe SM, Asef-Kabiri L, Yousefi H, et al. Cancer exosomes and natural killer cells dysfunction: biological roles, clinical significance and implications for immunotherapy. Mol Cancer 2022;21:15.
19. Takahashi N, Nishihira J, Sato Y, Kondo M, Ogawa H, Ohshima T, et al. Involvement of macrophage migration inhibitory factor (MIF) in the mechanism of tumor cell growth. Mol Med 1998;4:707-14.
20. Wong BL, Zhu S-L, Huang XR, Ma J, Xia HH, Bucala R, et al. Essential role for macrophage migration inhibitory factor in gastritis induced by Helicobacter pylori. Am J Pathol 2009;174:1319-28.
21. Nojima T, Proudfoot NJ. Mechanisms of lncRNA biogenesis as revealed by nascent transcriptomics. Nat Rev Mol Cell Biol 2022;23:389-406.
22. Herman AB, Tsitsipatis D, Gorospe M. Integrated lncRNA function upon genomic and epigenomic regulation. Mol Cell 2022;82:2252-66.
23. Shi X, Sun M, Liu H, Yao Y, Song Y. Long non-coding RNAs: a new frontier in the study of human diseases. Cancer Lett 2013;339:159-66.
24. Rao X, Liu X, Liu N, Zhang Y, Zhang Z, Zhou L, et al. Long noncoding RNA NEAT1 promotes tumorigenesis in H. pylori gastric cancer by sponging miR-30a to regulate COX-2/BCL9 pathway. Helicobacter 2021;26:e12847.
25. Thai P, Statt S, Chen CH, Liang E, Campbell C, Wu R. Characterization of a novel long noncoding RNA, SCAL1, induced by cigarette smoke and elevated in lung cancer cell lines.

Am J Respir Cell Mol Biol 2013;49:204-11.

26. Byun HJ, Yoon JH, Lee SK. LUCAT1 Epigenetically Downregulates the Tumor Suppressor Genes and in Gastric Cancer. Yonsei Med J 2020;61:923-34.
27. Yoon J-H, You B-H, Park CH, Kim YJ, Nam J-W, Lee SK. The long noncoding RNA LUCAT1 promotes tumorigenesis by controlling ubiquitination and stability of DNA methyltransferase 1 in esophageal squamous cell carcinoma. Cancer Lett 2018;417:47-57.
28. Cao Y, Zou Z, Wu X, Li W, Lu Z, Hu J, et al. LUCAT1 inhibits ferroptosis in bladder cancer by regulating the mRNA stability of STAT3. Gene 2024;894:147974.
29. Vierbuchen T, Agarwal S, Johnson JL, Galia L, Lei X, Stein K, et al. The lncRNA LUCAT1 is elevated in inflammatory disease and restrains inflammation by regulating the splicing and stability of NR4A2. Proc Natl Acad Sci U S A 2023;120:e2213715120.
30. Kuai X-y, Yu S-y, Cui X-f, Zhao X-j, Mao X-q, Yu Y, et al. LncRNA LUCAT1 as a plasma biomarker for assessing disease activity in adult patients with Crohn's disease. Gastroenterol Res Pract 2021;2021:5557357.
31. Fang F, Zhao M, Jin X, Dong Z, Wang J, Meng J, et al. Upregulation of MCL-1 by LUCAT1 through interacting with SRSF1 promotes the migration and invasion in non-small cell lung carcinoma. Mol Cell Biochem 2023:1-11.
32. Wang X, Guo S, Zhao R, Liu Y, Yang G. STAT3-activated long non-coding RNA lung cancer associated transcript 1 drives cell proliferation, migration, and invasion in hepatoblastoma through regulation of the miR-301b/STAT3 axis. Hum Gene Ther 2019;30:702-13.
33. Ran X-M, Yang J, Wang Z-Y, Xiao L-Z, Deng Y-P, Zhang K-Q. M2 macrophage-derived exosomal circTMCO3 acts through miR-515-5p and ITGA8 to enhance malignancy in ovarian cancer. Commun Biol 2024;7:583.
34. Gao N, Li Y, Li J, Gao Z, Yang Z, Li Y, et al. Long non-coding RNAs: the regulatory mechanisms, research strategies, and future directions in cancers. Front Oncol 2020;10:598817.
35. Chen W, Zuo F, Zhang K, Xia T, Lei W, Zhang Z, et al. Exosomal MIF derived from nasopharyngeal carcinoma promotes metastasis by repressing ferroptosis of macrophages. Front Cell Dev Biol 2021;9:791187.
36. Matsushita H, Yang YM, Pandol SJ, Seki E. Exosome migration inhibitory factor as a

marker and therapeutic target for pancreatic cancer. Gastroenterology 2016;150:1033-5.

37. Macías M, García-Cortés Á, Torres M, Ancizu-Marckert J, Pascual JI, Díez-Caballero F, et al. Characterization of the perioperative changes of exosomal immune-related cytokines induced by prostatectomy in early-stage prostate cancer patients. Cytokine 2021;141:155471.

38. Munson P, Shukla A. Exosomes: potential in cancer diagnosis and therapy. Medicines 2015;2:310-27.

39. Lu J, Xie L, Liu C, Zhang Q, Sun S. PTEN/PI3k/AKT regulates macrophage polarization in emphysematous mice. Scand J Immunol 2017;85:395-405.

40. Chen T, Liu Y, Li C, Xu C, Ding C, Chen J, et al. Tumor-derived exosomal circFARSA mediates M2 macrophage polarization via the PTEN/PI3K/AKT pathway to promote non-small cell lung cancer metastasis. Cancer Treat Res Commun 2021;28:100412.

41. Vergadi E, Ieronymaki E, Lyroni K, Vaporidi K, Tsatsanis C. Akt signaling pathway in macrophage activation and M1/M2 polarization. The Journal of Immunology 2017;198:1006-14.

42. Wang F, Li B, Wei Y, Zhao Y, Wang L, Zhang P, et al. Tumor-derived exosomes induce PD1+ macrophage population in human gastric cancer that promotes disease progression. Oncogenesis 2018;7:41.

43. Ma B, Wang J, Yusufu P. Tumor-derived exosome ElNF1-AS1 affects the progression of gastric cancer by promoting M2 polarization of macrophages. Environ Toxicol 2023;38:2228-39.

44. Xin L, Wu Y, Liu C, Zeng F, Wang J-L, Wu D-Z, et al. Exosome-mediated transfer of lncRNA HCG18 promotes M2 macrophage polarization in gastric cancer. Mol Immunol 2021;140:196-205.

45. Choi IJ, Kook M-C, Kim Y-I, Cho S-J, Lee JY, Kim CG, et al. Helicobacter pylori therapy for the prevention of metachronous gastric cancer. N Engl J Med 2018;378:1085-95.

46. Martianov I, Ramadass A, Serra Barros A, Chow N, Akoulitchev A. Repression of the human dihydrofolate reductase gene by a non-coding interfering transcript. Nature 2007;445:666-70.

47. Zhou X, Ao X, Jia Z, Li Y, Kuang S, Du C, et al. Non-coding RNA in cancer drug resistance: Underlying mechanisms and clinical applications. Front Oncol 2022;12:951864.

48. Zhu X, Tian X, Yu C, Shen C, Yan T, Hong J, et al. A long non-coding RNA signature to improve prognosis prediction of gastric cancer. Mol Cancer 2016;15:1-16.
49. Pauli A, Valen E, Lin MF, Garber M, Vastenhouw NL, Levin JZ, et al. Systematic identification of long noncoding RNAs expressed during zebrafish embryogenesis. Genome Res 2012;22:577-91.
50. Trapnell C, Williams BA, Pertea G, Mortazavi A, Kwan G, Van Baren MJ, et al. Transcript assembly and quantification by RNA-Seq reveals unannotated transcripts and isoform switching during cell differentiation. Nat Biotechnol 2010;28:511-5.
51. Hua-Xiang H, Lam S-K, Huang X-R, Wong W-M, Leung S-Y, Yuen S-T, et al. Helicobacter pylori infection is associated with increased expression of macrophage migratory inhibitory factor—by epithelial cells, T cells, and macrophages—in gastric mucosa. J Infect Dis 2004;190:293-302.
52. Luzón-Toro B, Fernández RM, Martos-Martínez J, Rubio-Manzanares-Dorado M, Antiñolo G, Borrego S. LncRNA LUCAT1 as a novel prognostic biomarker for patients with papillary thyroid cancer. Sci Rep 2019;9:14374.
53. Okazaki S, Boku S, Otsuka I, Horai T, Kimura A, Shimmyo N, et al. Clozapine increases macrophage migration inhibitory factor (MIF) expression via increasing histone acetylation of MIF promoter in astrocytes. J Psychiatr Res 2021;135:237-42.
54. Kouzarides T. Chromatin modifications and their function. Cell 2007;128:693-705.
55. Zhang C, Ge S, Gong W, Xu J, Guo Z, Liu Z, et al. LncRNA ANRIL acts as a modular scaffold of WDR5 and HDAC3 complexes and promotes alteration of the vascular smooth muscle cell phenotype. Cell Death Dis 2020;11:435.
56. Mills C. M1 and M2 macrophages: oracles of health and disease. Crit Rev Immunol 2012;32:463-88.
57. Feng R, Morine Y, Ikemoto T, Imura S, Iwahashi S, Saito Y, et al. Nrf2 activation drive macrophages polarization and cancer cell epithelial-mesenchymal transition during interaction. Cell Commun Signal 2018;16:1-12.
58. Zhang Y, Yan J, Li C, Wang X, Dong Y, Shen X, et al. LncRNA H19 induced by helicobacter pylori infection promotes gastric cancer cell growth via enhancing NF-κB-induced inflammation. J Inflamm 2019;16:1-8.
59. Pang Q, Ge J, Shao Y, Sun W, Song H, Xia T, et al. Increased expression of long intergenic

non-coding RNA LINC00152 in gastric cancer and its clinical significance. Tumour Biol 2014;35:5441-7.

60. Zhou X, Chen H, Zhu L, Hao B, Zhang W, Hua J, et al. Helicobacter pylori infection related long noncoding RNA (lncRNA) AF147447 inhibits gastric cancer proliferation and invasion by targeting MUC2 and up-regulating miR-34c. Oncotarget 2016;7:82770.

Appendix

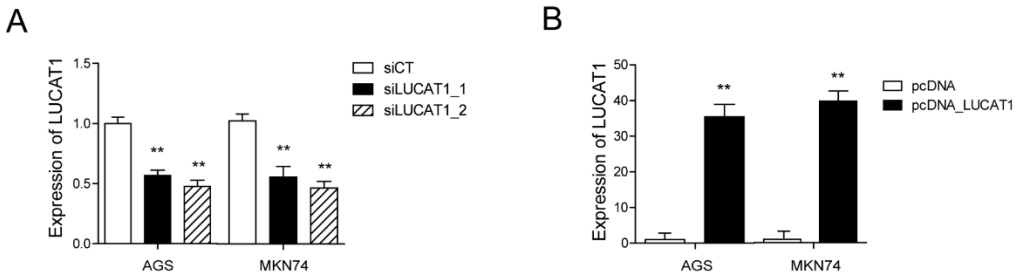

Figure S1. Expression of LUCAT1 in GC cells transfected with siLUCAT1s and pcDNA_LUCAT1. **(A)** LUCAT1 expression in AGS and MKN74 cells transfected with a siControl or siLUCAT1s was measured by qRT-PCR. **(B)** LUCAT1 expression in AGS and MKN74 cells transfected with a pcDNA or pcDNA_LUCAT1 was measured by qRT-PCR. All of the data are from three independent experiments. Data represented the mean ± s.e.m. $n = 3$, t test, $*P < 0.05$, $**P < 0.01$, $***P < 0.001$ versus con group.

Abstract in Korean

위암에서 *Helicobacter pylori* 감염에 의해 유도된 lncRNA LUCAT1의 exosomal MIF 조절을 통한 M2 대식세포 분극화

헬리코박터 파일로리(*Helicobacter pylori*, *H. pylori*)는 위염, 소화성 궤양 질환 및 위암 발병의 주요 병인으로 잘 알려져 있다. 한편, 200개 이상의 뉴클레오타이드로 구성된 긴 비번역 RNA(long noncoding RNA, lncRNA)는 다양한 암, 특히 위암의 발생과 진행에서 중요한 역할을 하는 것으로 인식되고 있다. 염증 반응, 예를 들어 *H. pylori* 감염에 의해 유발되는 암 발달에 lncRNA가 관여하는 것은 알려져 있으나, *H. pylori* 감염에 의해 유도되는 lncRNA 발현 변화에 대한 이해는 여전히 제한적이다. 이를 해결하기 위해 본 연구에서는 *H. pylori*의 병리학적 인자인 세포 독소 관련 유전자 A(CagA)를 고려하여 정상 및 위암 세포에서 *H. pylori* 감염 후 lncRNA와 유전자 발현 변화를 분석하고, *H. pylori* 감염에 의한 위암 진행에 기여하는 lncRNA를 확인했다. RNA 시퀀싱과 후속 검증 연구를 통해 LUCAT1이 CagA 양성 *H. pylori*에서 현저히 상향 조절됨을 확인하였다. LUCAT1 발현 증가는 이어서 엑소좀을 통해 분비되는 대식세포 이동 억제 인자(MIF)의 발현을 높였으며, 이는 종양 관련 대식세포의 M2 분극화를 촉진하여 위암 세포의 악성화를 강화했다. 본 연구는 *H. pylori* 감염이 lncRNA 발현 및 엑소좀 매개 신호 전달 조절을 통해 종양 미세환경에 미치는 영향을 확인하였고, 위암 진행에서 lncRNA 기반 기전의 중요성을 보여준다. 이를 통해, 위암 발생 예방을 위한 방법으로 *H. pylori*의 완전한 박멸만을 목표로 하는 기존 접근법에서 벗어나 lncRNA 조절 및 엑소좀 신호 전달을 표적으로 하는 새로운 치료 전략을 탐구할 기회를 제공한다.

핵심되는 말 : 헬리코박터 파일로리, CagA, 긴 비번역 RNA, LUCAT1, MIF, 대식세포, 엑소좀, RNA 시퀀싱, 위암